Extraction of blufflines from 2.5 dimensional Delaunay triangle mesh using LiDAR data

Thesis

Presented in the Partial Fulfillment of the Requirements for the Degree Master of Science in the Graduate School of The Ohio State University

By

YUNJAE CHOUNG, B.E.

Graduate Program in Geodetic Science and Surveying

The Ohio State University

2009

Thesis Committee:

Dr. Rongxing Li, Advisor

Dr. Alper Yilmaz

ABSTRACT

Bluffline mapping is critical for estimation of shoreline movement, development of coastal zone, and protection of coastal properties and coastal environment. LiDAR technology has been utilized in coastal mapping since the late 1990's. Research on development of the method for bluffline extraction using LiDAR data has been carried out very recently. The method for bluffline extraction from LiDAR DSM by analysis of slope values (termed as the slope based method) was developed in the Mapping and GIS lab of OSU. The slope based method was applied to extract the blufflines in the coastal zone of Lake Erie. This method has theoretical limitations with analysis of the geometric patterns; hence it does not provide enough information for extraction of blufflines due to the limitations. In addition, the slope based method requires manual labor to extract the three dimensional blufflines. In this thesis, a method for bluffline extraction from the 2.5 dimensional Delaunay triangle mesh, generated using a set of points of LiDAR, using normal vectors (termed as the vector based method) is introduced. This vector based method is also applied to extract the blufflines in the coastal zone of Lake Erie. This thesis proves that the vector based method provide more information for extraction of blufflines in comparison to the slope based method.

Introduction to the definition of blufflines, introduction of the slope based method and statements of current problems for bluffline extraction are the first theme of this thesis. Introduction to the vector based method for bluffline extraction is the second theme of this thesis. Introduction to the coastal zone of Lake Erie and all implementations of the vector based method for bluffline extraction are the third theme of this thesis. Measurement of accuracy of the blufflines extracted using both methods and analysis of both methods with the measurement results are the fourth theme of this thesis. Summarization of conclusions of this research and future work for further research for bluffline extraction with a high quality using surveying data are the final theme of this thesis.

Dedicated to my family,

Dr. Yunsoo Choung, Dr. Myunghee Jo

and Ms. Mihwa Choung

ACKNOWLEDGEMENTS

FIELDS OF STUDY

Graduate Program: Geodetic Science and Surveying

Department: Civil and Environmental Engineering and Geodetic Science

Concentration: Mapping and Geographic Information System

Table of Contents

List of Figures

xi

List of Tables

List of Abbreviation

ATM   Airborne Topographic Mapper

DSM   Digital Surface Model

GCPs   Ground Control Points

GIS   Geographic Information Science

GPS   Global Positioning System

IMU   Inertial Measurement Unit

LiDAR   Light Detection and Ranging

NOAA   National Oceanic and Atmospheric Administration

ODNR   Ohio Department of Natural Resources

OSU   Ohio State University

RMSE   Root Mean Square Error

CHAPTER 1: INTRODUCTION

1.1 Background

Coastal mapping is essential for management of coastal resources, protection of coastal environments, and planning and development of coastal zones. Historically, coastal mapping has been carried out using surveying technologies. Photogrammetry, one of the surveying technologies, is the most popular and frequently used technology for national coastal mapping. In previous distinguished research, airborne LiDAR data has been used for coastal management due to its capability to penetrate shallow water (Wright and Brock, 2002; Mayer et al., 2004; Wozencraft and Millar, 2005). In addition, LiDAR data has high vertical accuracy (Ma, 2004). Due to these advantages, utilization of LiDAR data in coastal mapping is efficient for monitoring and predicting significant topographic change in coastal zones.

1.2 Definition of blufflines

A coastal bluff is a naturally formed precipitous landform and is generally considered to be composed of unconsolidated rock (Buonaiuto and Bokuniewicz, 2005). There are various elements which constitute a coastal bluff region. Figure 1.1 shows all elements which constitute a coastal bluff region.
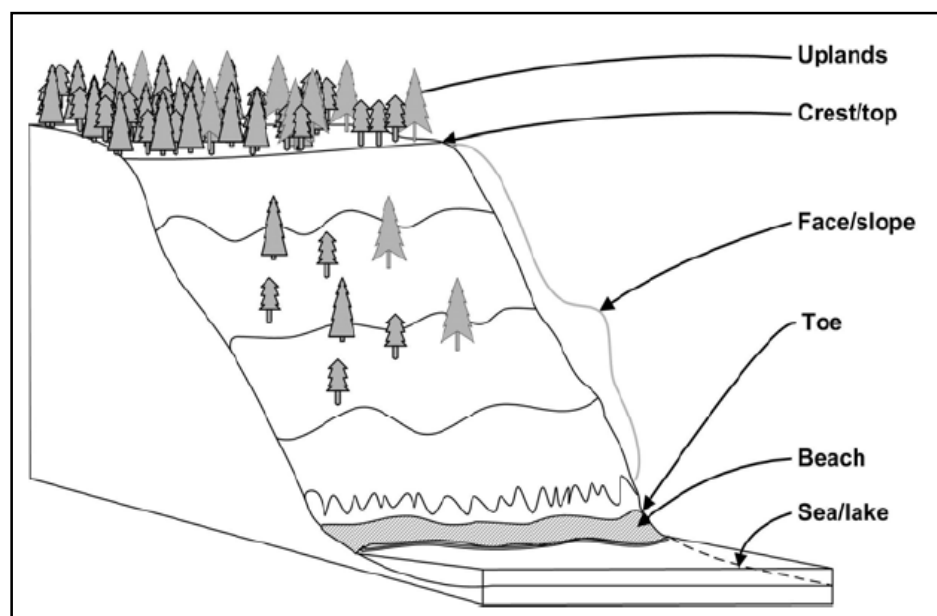
Figure 1.1 Elements of coastal bluff region (Adapted from Liu et al., 2009)

Blufflines are features which are generated in coastal bluff regions. In this research, both bluff top and bluff toe lines are defined as blufflines. The bluff top is defined as the crest edges of the upper segment above the beach that usually has a sharp front inclining steeply down to the side towards the water (California Coastal Commission, 2004). The bluff toe is defined as the base of a bluff where it meets the beach (Washington State Department of Ecology, 2009).

1.3 Difference between shoreline and bluffline

In general, blufflines are features which are very similar to shorelines. However, in some areas, blufflines are definitely distinguished from shorelines. Definition of shoreline is explained below.

1) "the line of contact between the land and a body of water" (Shalowitz, 1964)

2) "…the intersection of the land with the water surface" (Gill and Schultz, 2001)

The shoreline is equivalent to the bluffline in the areas where there is no bluff standing on the lakeshore (or seashore) or where the water body directly contacts the bottom of bluffs (Liu et al., 2009). In this region, the shoreline is approximated to the bluffline.

However, in some coastal regions, e.g., sandy beach regions, where coastal erosion is serious, the bluff stands on hundreds of feet away from the shoreline due to coastal erosion (Liu et al., 2009). In this region, the blufflines moves landward and are definitely distinguished from the shoreline.

1.4 Influence of coastal erosion and need for bluffline mapping

Erosion is defined as the gradual wearing away of the earth's surface by the action of the natural forces of wind and water (Li et al., 2001). In general, erosion in coastal zone is termed as coastal erosion. Coastal erosion causes damage to the ecosystem of a coastal region. Damage to the coastal ecosystem causes drastic change not only in under-water life, but also in human life in the coastal zone. Coastal erosion raises a big problem for coastal communities in their daily activities like navigation, coastal zone management, coastal environmental protection, and sustainable development (Srivastava, 2005).

Coastal erosion causes negative effects on land property, beach and structure near the shore (Fletcher et al., 2003; Li, 1997). Coastal erosion is one of the main factors of constant change of shorelines around lakes or oceans.

Two factors are essential in describing coastal erosion: one is the breaking waves in the near shore zones and the other is the near shore currents (Ali, 2003). The breaking waves in the near shore zones and the near shore currents transport coastal sediments such as soils and rocks from one part to another part, which result in topographic change and littoral transport in coastal zone (Ali, 2003).

These two factors also results in bluff erosion. Figure 1.2 shows the cycle of bluff erosion.
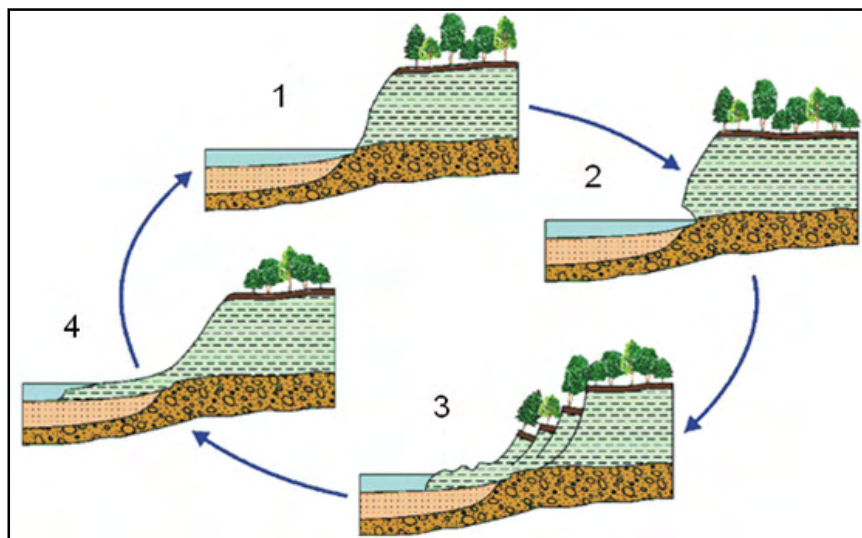
Figure 1.2 The cycle of bluff erosion (Modified from Maine geological survey, 2009)

In Figure 1.2, the waves remove the exposed bluff materials and undercut the bluff toe (from 1 to 2). Wave breaking is a highly nonlinear phenomenon, and it is important to

describe the phenomenon analytically (Chopakatla et al., 2008). In areas where the coastal bluff consists of clay with a thickness of 20 feet or more (3), there is a risk of internal failure and down slope movement in the form of a landslide (Maine geological survey, 2009). Large, deep-seated slumps locally occur, depositing the material at the base of bluff. Then the waves restart their direct attack (4) on the intact bluff face, and, eventually, another large, deep-seated slump occurs. Such wave erosion prevents the bluff slopes from ever attaining equilibrium (Brown et al., 2005).

Coastal erosion generally occurs within an area roughly from the bluff crest out into the near shore to the water depth of about 30 feet, and bluff recession is the most visible aspect of coastal erosion (Liu, 1998). Thus, periodical bluffline mapping is essential for prediction of coastal erosion, determination of coastal boundaries, monitoring of topographic change in coastal region, estimation of volume of soil loss in bluff region and management of coastal zone.

Although there is significant difference between the shoreline and the bluffline, in some coastal studies, the bluff top edge is chosen as the shoreline indicator due to its easy visibility on aerial photographs (Srivastava, 2005). Hence, bluffline mapping is also useful for shoreline mapping.

1.5 The basic principle of LiDAR

LiDAR is an active sensor which transmits the laser pulses to a target and records the time it takes for the pulse to return to the sensor receiver (NOAA, 2009). LiDAR is one of the surveying technologies belonging to the scope of photogrammetry; however,

LiDAR may be considered as a separate surveying technology different from photogrammetry due to its characteristics (Ma, 2004). The results of LiDAR are the 3D coordinates of the measured points on the object surface, while the results of photogrammetry are imagery data.

Several technologies including the LiDAR sensor are operated in a LiDAR system to obtain high accuracy point data on the object surface. In a LiDAR system, GPS is used to determine the X, Y and Z coordinates of the moving LiDAR sensor, and IMU is used to establish the angular orientation of the LiDAR sensor about the X, Y and Z axis in flight. Figure 1.3 shows operation of Airborne LiDAR system.
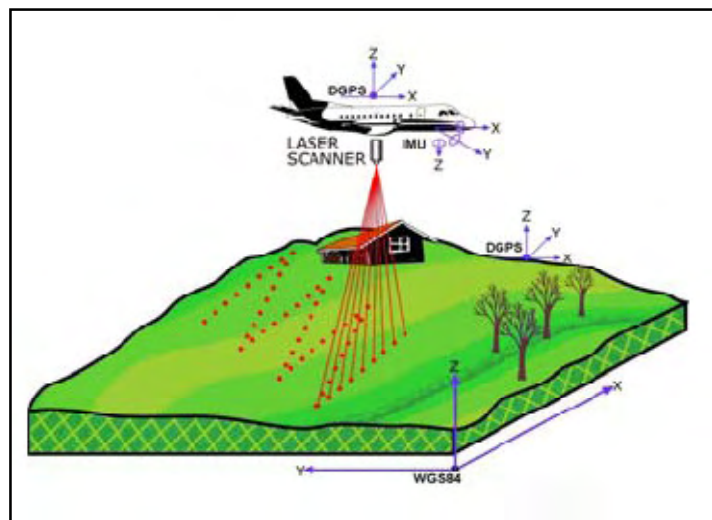
Figure 1.3 Operation of Airborne LiDAR system

In a LiDAR system, the laser pulses are used to measure the distance from the LiDAR sensor to an object. The LiDAR sensor emits the laser pulse, and the laser pulse is reflected from the surface of objects. The LiDAR system records the travel time of the

6

laser pulse by measurement of the time difference between emission of the laser pulse and reception of the reflected laser pulse in the LiDAR instrument.

Table 1.1 displays the major specifications for LiDAR mapping technology (NOAA, 2009). Standard specifications were collected from the various LiDAR sensors which are frequently used. These specifications may not apply to all LiDAR sensors.

Pulse Rate	≤ 40 KHz
Wavelength	1.045 - 1.065 µm (near infrared)
Altitude	300 - 2000 meters
Swath Width	Up to 0.70 × altitude (meters)
Z Accuracy (Vertical) RMSE	Approximately 15 centimeters
X, Y Accuracy (Horizontal) RMSE	≤ 1 meter
Resolution (point spacing)	≥ 0.75 meters
Laser Footprint on ground	≤ 0.50 meters

Table 1.1 Specification of the typical LiDAR system (NOAA, 2009)

The distance from the transmitter to the object would be determined by using the accurate travel time of the laser pulse. The distance from the transmitter to the object can be computed using equation 1.1. In equation 1.1, T_l is travel time of laser, D is the distance from the transmitter to the object and v is the speed of laser.

$$D = \frac{v \cdot T_l}{2} \tag{1.1}$$

The LiDAR sensor collects the point data using a scanning mirror, which includes linear and conical scanners, and the sensor measures the scan angle of the laser pulse.

LiDAR technology can offer high point data density. Point density is an important factor of LiDAR data. Point density means the average ground spacing of a set of points, the result of the LiDAR surveying. The point density of LiDAR data is determined by flying height, the scan angle, scan pattern, and velocity, etc. In general, as scan angle is getting larger, the point density is getting lower, and as flying height is getting higher, the point density is also getting lower.

The positional accuracy and orientation parameters of the LiDAR system are determined by an integrated GPS/IMU. In general, the LiDAR data has high vertical accuracy of 15 ~ 30 cm or even better, and its horizontal accuracy varies according to horizontal resolutions (Ma, 2004).

LiDAR can be utilized for measurement of water depth, since the laser pulse can penetrate shallow water due to characteristics of its reflectance. The maximum depth penetration for a LiDAR system is dependent on water clarity, water turbidity and bottom reflection, etc.

1.6 Utilization of LiDAR data in coastal mapping

Surveying with LiDAR has many advantages in comparison to other technologies such as GPS, photogrammetry and land surveying. First of all, LiDAR technology is a more cost effective method for data collection than other surveying technologies. In addition, using LiDAR technology, three dimensional coordinates can be directly obtained, while multiple image matching processes are required to obtain three dimensional coordinates using traditional photogrammetry.

LiDAR data has been widely used in coastal mapping (Brock et al., 2002; Harris et al., 2005). Multiple reasons for utilization of LiDAR in coastal studies are explained below.

1) Using a LiDAR system, coastal lines over 100 km in length can be easily extracted within a three to four hour period (Liu et al., 2009). Hence, LiDAR technology is especially efficient for surveying accurately and rapidly morphologically dynamic areas such as beach areas.

2) Since LiDAR provides data with high vertical accuracy and has the ability to penetrate shallow water, using LiDAR data is useful for research of change detection or change analysis in coastal zone.

3) LiDAR is especially more useful for coastal areas than other surveying methods, since these coastal areas are featureless terrain. In general, the featureless terrain, e.g., coastal areas, restricts utilization of photogrammetry due to absence of GCPs. Only a few GCPs are needed in surveying with LiDAR technology due to differential GPS theory. Hence, utilization of LiDAR technology is ideal for mapping of featureless areas, e.g., coastal areas.

1.7 Utilization of aerial orthoimage in bluffline mapping

Utilization of aerial orthimages alone for bluffline mapping results in occlusions introduced by vertical features including trees or shadows and would often affect determination and identification of the positions of the bluff toe and the bluff top. In this research, the aerial orthoimages are just used as reference surfaces to determine the ground truths needed for measurement of accuracy of the blufflines extracted using two

methods. Figure 1.4 shows the manually digitized bluff toe line (the yellow line) and bluff top line (the red line) from the aerial orthoimages used as reference surfaces in this research.

Figure 1.4 Digitized bluff top line and bluff toe line from the aerial orthoimage

1.8 Literature Review

1.8.1 Introduction

Research on feature change analysis caused by coastal erosion has been carried out: Liu (1998) developed the GIS model to analyze shoreline change due to coastal erosion for erosion control on the Lake Erie shoreline; Ali (1999) developed the GIS model to estimate soil loss due to coastal erosion in coastal zone of the Lake Erie. Ali (2003) also developed shoreline change modeling based on shoreline segment orientation for better

analysis of shoreline change at the segment level by studying the angular deviation from the surrounding segments and also from the whole shoreline.

Research on bluffline mapping for prediction of coastal erosion and shoreline mapping has been carried out: Srivastava (2005) developed the bluffline analytical model for analysis of shorelime movement and coastal erosion. A bluffline is divided into a finite number of segments, and the least squares approach with transformation parameters is used to predict the movement of the bluffline segments. The future blufflines can be easily derived using the least squares approach with transformation parameters.

Bluffline extraction using remote sensing data is useful for prediction of coastal erosion and estimation of the movement of blufflines with higher accuracy. Research on the development of methods for extraction of blufflines using the remote sensing data has been carried out: Liu et al. (2009) developed a new method for bluffline extraction from the LiDAR DSM by analysis of slope values (termed as the slope based method). Using this method, the bluff top and toe points are extracted from each three dimensional profile, generated along a transect obtained from the LiDAR DSM. These bluff top and toe points are connected across transects to form initial three dimensional blufflines. The edges obtained from the aerial orthoimages using techniques including edge detection, mean-shift segmentation and surface reconstruction are used to refine the horizontal position of the initial blufflines. The refined blufflines have a similar quality to the manually digitized blufflines.

Blufflines are similar to structure lines or breaklines. Research on detection of breaklines using image processing technologies has been carried out: Brügelmann (2000) developed

a method for automatic detection of breaklines using gray-value images which represent the range of LiDAR data. A hypothesis method was employed for identification of the breaklines. Thinning of the initial broad blufflines was implemented by non-maxima suppression. After the thinning process, the breaklines were vectorized and a spline function was fitted through the X and Y coordinates of them. Briese (2004) proposed a method for modeling three dimensional breaklines using LiDAR data. The three dimensional position of a breakline was estimated by the intersection of two planes; a plane was located on either side of the breakline. LiDAR data was divided into two regions using an initial approximation of the breaklines. Each divided region was fitted with a plane. The intersection of two planes was employed as a new approximation of the breakline. This process was repeated until a stable breakline was obtained. After the approximation process, a spline function was fitted through the three dimensional points for representation of the final breakline.

Research on the development of methods for extraction of features from triangle meshes with computation of normal vector of each triangle has been carried out: Hubeli and Gross (2001) developed a method for extraction of linear curves from unstructured triangle mesh with computation of normal vectors; Page et al. (2002) developed the method for crease detection and curvature estimation from large and noisy triangle mesh with computation of normal vectors.

Extraction of specific features from the Delaunay triangle mesh has the wide range of applications. Bebis et al. (1999) proposed a method for identification of fingerprint using the Delaunay triangulation. Tse et al. (2007) developed a method for extraction of

building shape from the Delaunay triangle mesh generated using a set of points of LiDAR

for three dimensional city modeling.

1.8.2 A method for bluffline extraction from LiDAR DSM by analysis of slope values

The primary objective of this thesis is to propose an improved method for bluffline

extraction using remote sensing data in comparison to the slope based method. Before the

improved method is proposed, this section reviews the slope based method for bluffline

extraction using LiDAR data. Figure 1.5 presents the flow diagram showing the process

of the slope based method.
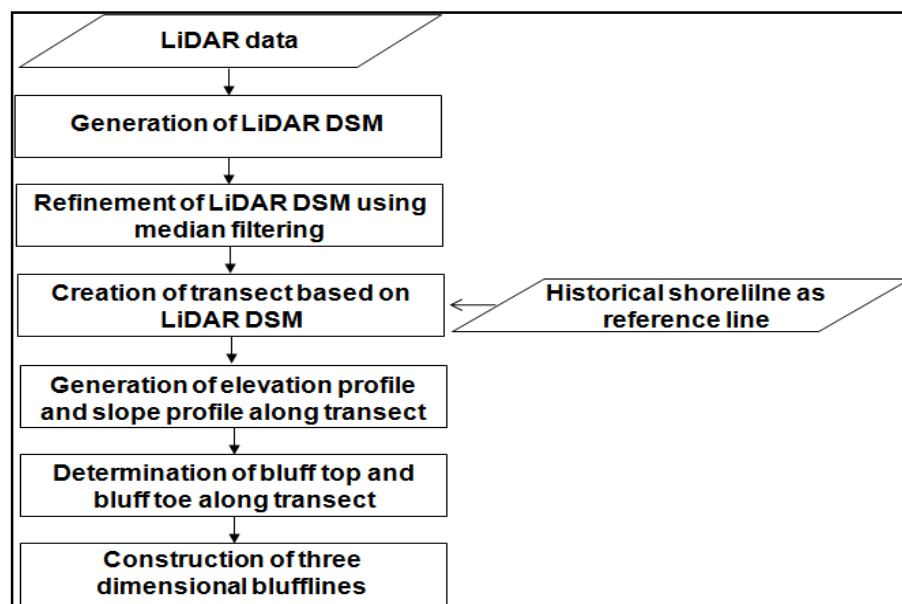
Figure 1.5 Flow diagram showing the process of the slope based method (Liu et al., 2009)

A historical bluff line is used as a reference line (the red line in Figure 1.6) to create a

series of transects (the yellow lines in Figure 1.6), and each generated transect is

perpendicular to the reference line. The average distance between the transects is 30m (Liu et al., 2009). Three dimensional elevation profiles are generated along transects based on the LiDAR DSM. Figure 1.7 presents a three dimensional elevation profile generated along a transect.
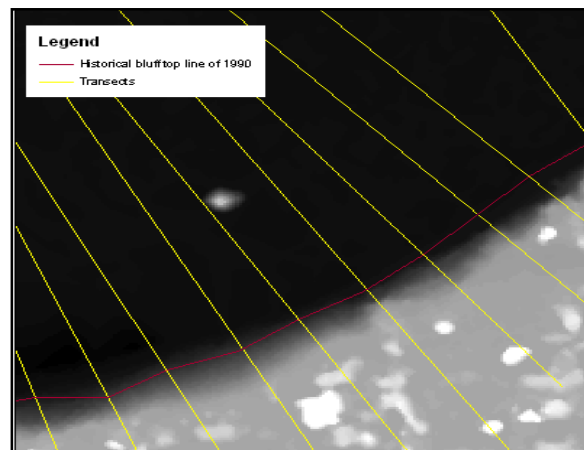
Figure 1.6 Transects perpendicular to the reference line
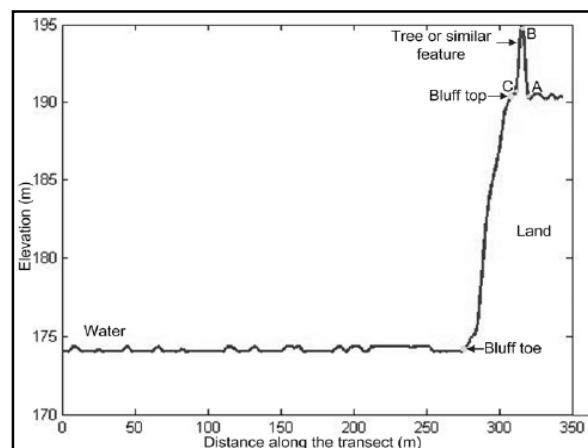
Figure 1.7 Three dimensional elevation profile generated along a transect
(Adapted from Liu et al., 2009)

14

In Figure 1.7, a sequence of linearly interpolated points, generated from the LiDAR DSM, constitute a three dimensional elevation profile with a uniform spacing d. Along each three dimensional elevation profile, the bluff top and toe points can be determined by analysis of the elevation information of these interpolated points. For analysis of the elevation information of these interpolated points, slope value of each interpolated point should be obtained to generate a slope profile (Liu et al., 2009). The slope value at Point i, at m different scales is defined as:

$$BSlope_i^j = \frac{H_{i+1} - H_{i-j+1}}{j \cdot d} \qquad (1.2)$$

In above equation 1.2, j is the point index interval from Point i toward the water, and H_i is the elevation at Point i. In this research, $j = 10$ is used to obtain a smoother profile and reduce influence of noises, and $d = 0.5$ m is used as a uniform spacing to preserve the details of the LiDAR data. Figure 1.8 presents a slope profile with $j = 10$ and $d = 0.5$ m of the elevation profile shown in Figure 1.7.
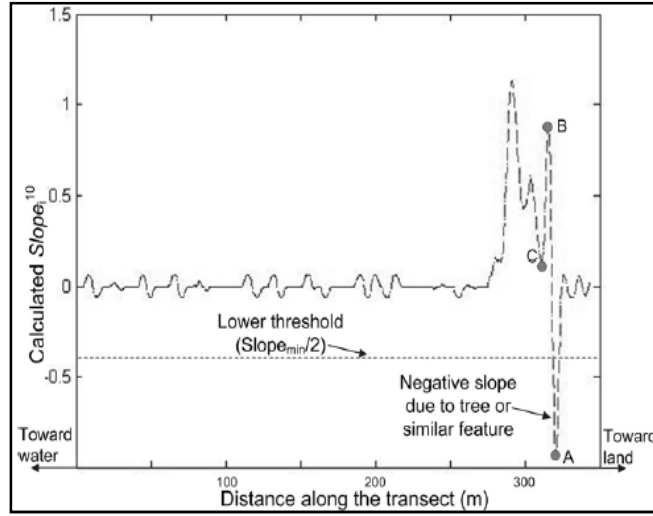
Figure 1.8 Slope profile with $j = 10$
(Adapted from Liu et al., 2009)

All the points which constitute the vertical features in the elevation profile are removed by analysis of slope value ($BSlope_i^{10}$) of the interpolated points. After elimination of all the points which consist of vertical features, determination of the bluff top and toe points along each transects is carried out.

1) Determination of the bluff top point

The maximum slope ($BSlope_{max}$) along the slope profile and a slope constraint (SC) should be defined to determine the bluff top point. The slope constraint (SC) is defined as SC = $BSlope_{max}$/4, and the points satisfying the conditions ($BSlope_i^{10} \geq SC$, $BSlope_i^{10} \geq BSlope_{i+1}^{10}$) are defined as the multiple bluff top candidates in the elevation profile (Liu et al., 2009). Among the multiple bluff top candidates, the point with maximum elevation is defined as the bluff top point in the elevation profile.

16

2) Determination of the bluff toe point

The bluff toe point can be defined in the reversed elevation profile using the same method used to determine the bluff top point in the elevation profile. Among the multiple bluff toe candidates, the point with maximum elevation is defined as the bluff toe point in the reversed elevation profile.

Figure 1.9 presents the locations of the bluff top and toe points in the elevation profile.
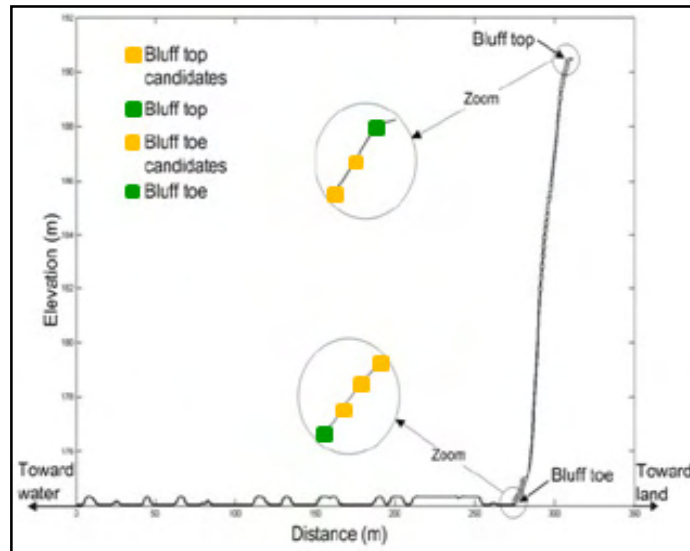
Figure 1.9 Locations of the bluff top and toe points in the elevation profile
(Adapted from Liu et al., 2009)

17

After the bluff top and toe points are identified in the three dimensional elevation profile, the three dimensional blufflines are generated by connecting each bluff top point and bluff toe point across the transects. Figure 1.10 shows the three dimensional blufflines (the blue lines), extracted using the slope method, by connecting each bluff top point and bluff toe point (the blue points) across the transects (the yellow lines).
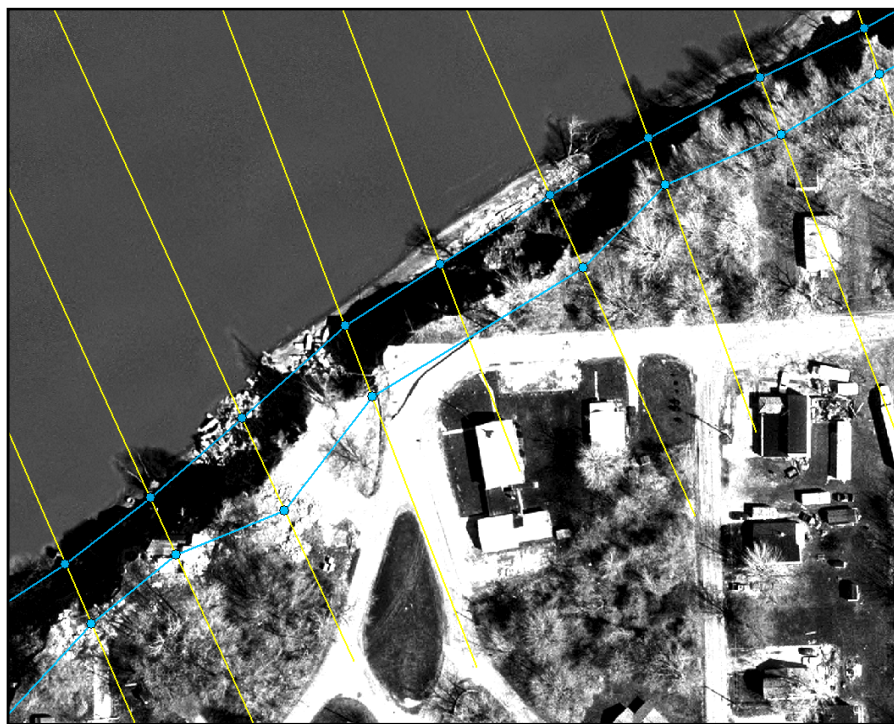
Figure 1.10 Blufflines extracted using the slope based method

1.9 Problem statements

This section discusses the need for development and improvement of the method for bluffline extraction.

1) Manual digitization of blufflines is a highly time consuming work due to the total length of blufflines in the coastal zones of the United States. In addition, manual digitization is affected by oerator judgment and cause random errors due to misinterpretation. Hence, a method for automatic extraction of blufflines is needed for minimization of manual interaction, effectiveness of coastal mapping, and effective management of coastal zone.

2) The slope based method has theoretical limitations to detect the bluff top and toe points. This method analyzes geometric patterns to extract blufflines only in a single direction; while the locations of blufflines are affected by three dimensional geometric patterns. Thus, this method does not provide enough information to detect the bluff top and toe lines due to its analysis of geometric patterns. In addition, since the bluff top and toe points are only identified along each transect, this method requires huge amount of manual labor, including the creation of numerous number of transects and linking the bluff top and toe points across transects, for creation of the three dimensional blufflines. Hence, another method for extraction of blufflines using LiDAR data is needed to extract the three dimensional blufflines.

1.10 Objective and methology

The ultimate goal of this research is to propose a new method (vector based method) for the three dimensional bluffline extraction using LiDAR data with more automatic processes and higher quality in comparison to the slope based method.

The 2.5 dimensional Delaunay triangle mesh is generated using a set of LiDAR points, and a median filter is applied to remove noises and small vertical features. The normal vector of each triangle is obtained, and two methods are employed to compute angle values defined by two normal vectors. Using two methods, each edge has two different angle values corresponding to each method. Hypothesis testing is employed for determination of the range of angle values in which important edges, including the bluff edges, can be well extracted. Using two methods, edges are separately extracted at the same range. Intersection edges, which are extracted using both methods at the same range, are selected. Using simple geometric algorithms, unsuitable edges for the bluffline segments are removed from the intersection edge group, and numerous line segments are extracted. With all the line segments located at the bluff top and the bluff toe, the three dimensional blufflines are generated by linking the end points of these line segments.

The vector based method analyzes three dimensional geometric patterns to extract the three dimensional blufflines. Using the method, numerous bluffline segments are extracted, and they are connected to each other for construction the three dimensional blufflines; hence, the three dimensional blufflines can be efficiently extracted using the method with little manual work. Thus, the vector based method is a more efficient method for bluffline extraction in comparison to the slope based method.

1.11 Organization of the thesis

This thesis is organized in five chapters as follows. Chapter 1 introduces the definition of blufflines, and reviews the slope based method. Chapter 2 introduces the vector based method for bluffline extraction. Chapter 3 describes the study area for this research, the data sets used in this research and implementation of all processes for this research. Chapter 4 presents the measurement results of accuracy of the blufflines extracted using both methods and analysis of both methods with the measurement results. Chapter 5 summarizes the conclusions of the research and illustrates the topics for future research.

CHAPTER 2: A METHOD FOR BLUFFLINE EXTRACTION FROM 2.5 DIMENSIONAL DELAUNAY TRIANGLE MESH USING NORMAL VECTORS

2. 1 Introduction

This chapter introduces a method for bluffline extraction from the 2.5 dimensional Delaunay triangle mesh, constructed using a set of points of LiDAR, using normal vectors (the vector based method). Figure 2.1 presents a flow diagram showing the process of the vector based method for bluffline extraction. Multiple steps are involved in the vector based method. The 2.5 dimensional Delaunay triangle mesh is generated using a set of point of LiDAR, and the triangle mesh surfaces are refined by a median filter. Considering angle values defined by two normal vectors, extraction of important edges including the bluff edges is implemented. Two methods are employed for extraction of important edges using two normal vectors. The range of angle values in which the important edges are well extracted is determined using hypothesis testing. Intersection edges, which are extracted using both methods at the same range, are chosen.

Considering connectivity, vertical distance and slope of an edge, most feature edges, unsuitable to compose the bluffline segments, are removed from the intersection edge group and line segments are extracted. With the extracted line segments located at the bluff top and the bluff toe, these line segments are connected to each other to construct the three dimensional blufflines.
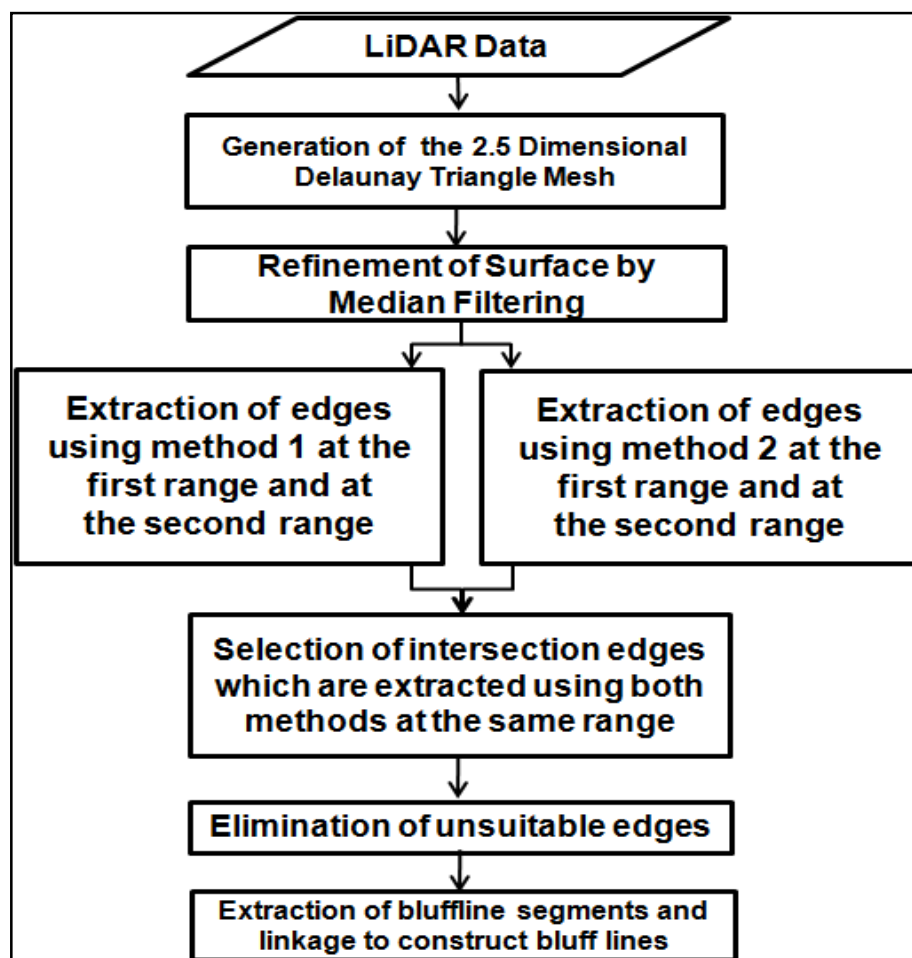
Figure 2.1 Flow diagram showing the overview of the process of the vector based method

2. 2 Generation of 2.5 dimensional Delaunay triangle mesh using the LiDAR data

This section discusses generation of the 2.5 dimensional Delaunay triangle mesh using

LiDAR data. Delaunay triangulation is defined as the set of lines joining a set of points

together such that each point is joined to its nearest neighbors (O'Rourke, 1993).

Delaunay triangulation is the most natural method to construct triangles with a set of

points. Figure 2.2 shows Delaunay triangulation with a set of points {p1…p10}.
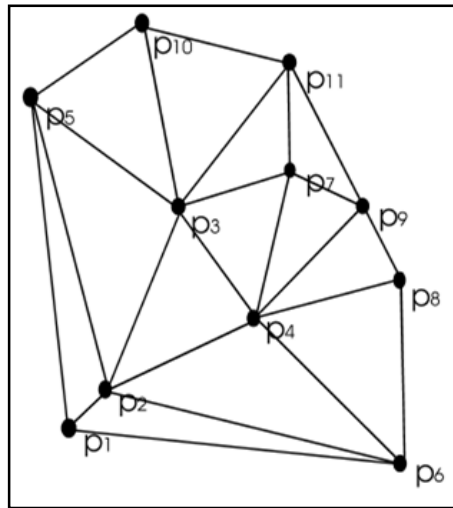
Figure 2.2 Delaunay triangulation with a set of points
(Adapted from Mulchrone, 2002)

The result of airborne LiDAR data is a set of points which consist of X, Y, and Z

coordinates. All point of LiDAR data are scattered on the surface of the Earth. Using the

three nearest three neighbor points of LiDAR data, the 2.5 dimensional Delaunay triangle

mesh can be generated. The 2.5 dimensional Delaunay triangle mesh can be also

generated using all the points of LiDAR data. Figure 2.3 presents one segment of the 2.5

24

dimensional Delaunay triangle mesh using the LiDAR data of the Lake Erie, Painesville, Ohio dataset.
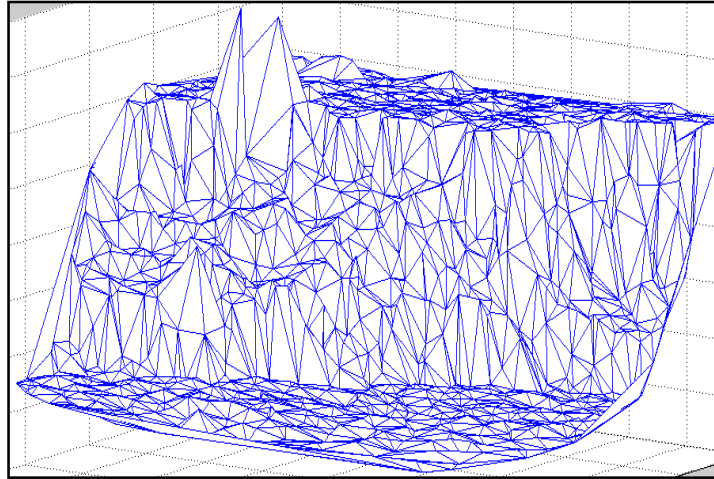
Figure 2.3 One segment of the 2.5 dimensional Delaunay triangle mesh using the LiDAR data of the Lake Erie, Painesville, Ohio dataset

2. 3 Refinement of surface of the triangle mesh using a median filter

In general, LiDAR data often include noise, and this noise is significantly inaccurate in comparison to other near points. This noise is generally caused by the LiDAR instruments.

Such noise can be minimized by filtering. In this research, a median filter is used to minimize this noise. Unlike the other filters such as a mean filter or a Gaussian filter, etc., the median filter is non-linear filter and is based on neighborhood ranking (Schenk, 1999). The points in the neighborhood are ranked according to their Z coordinates, then the median value in the sorted list is used as a representative elevation for the central point.

One of the major advantages of the median filter over other linear filters is that the median filter is well suited to eliminate a noisy point which has an extremely larger value in the neighborhood (Schenk, 1999). Other linear filters are generally sensitive to such noisy points. In addition, the median filter does not create unrealistic new points (Liu et al., 2009).

Figure 2.4 illustrates the result showing refinement of the 2.5 dimensional Delaunay triangulation surfaces using a median filter. Figure 2.4(a) shows the 2.5 dimensional Delaunay triangle mesh using the raw LiDAR data. The spikes, in Figure 2.4(a), show noises in the raw LiDAR data. The segment of the refined 2.5 dimensional Delaunay triangle mesh after using a median filter is shown in Figure 2.4(b).

(a) The 2.5 dimensional Delaunay triangle mesh using the raw LiDAR data	(b) The refined 2.5 dimensional Delaunay triangle mesh after elimination of spikes using a median filter
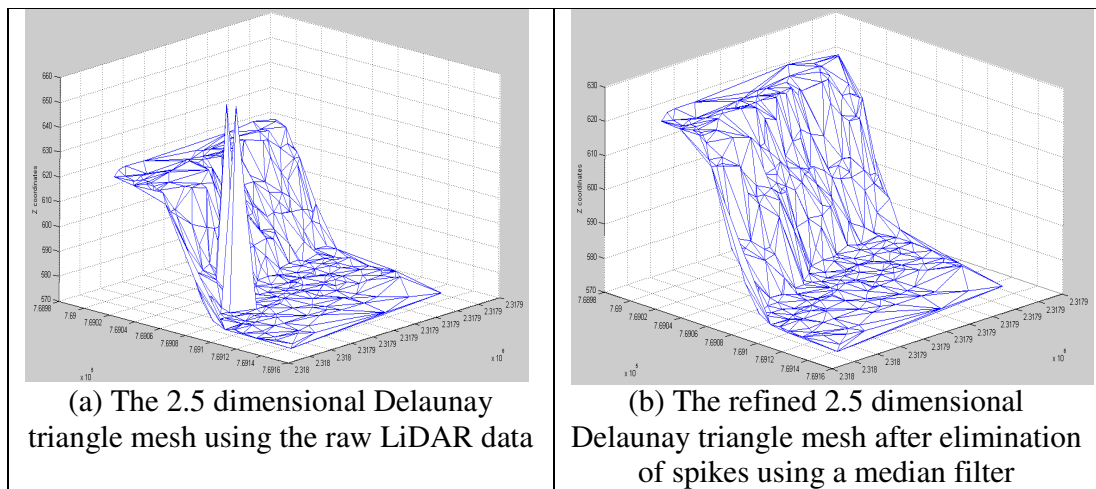
Figure 2.4 Result showing refinement of the 2.5 dimensional Delaunay triangle mesh using a median filter

2.4 Extraction of edges using two methods

The objective of this step is to extract important edges, which include the bluff edges, from the 2.5 dimensional Delaunay triangle mesh using two methods. Using two methods, angle values defined by two normal vectors can be assigned to an edge. Each method has its own way to assign an angle value to each edge; hence, each edge has two different angle values computed by two different methods. Both methods have been employed to extract linear features from the triangle mesh (Hubeli and Gross, 2001). The equation used in method 1 to assign an angle value to each edge is defined as:

$$A_1(e) = \text{arc} \cos \left(\frac{n_i}{\|n_i\|} \cdot \frac{n_j}{\|n_j\|} \right) \tag{2.1}$$

where e is an edge in the Delaunay triangle mesh, $A_1(e)$ is a dihedral angle value defined by two normal vectors of two adjacent triangles which share the edge e, the variables n_i , n_j are defined as normal vectors of two adjacent triangles which share the edge e, and the variables $\|n_i\|$, $\|n_j\|$ correspond to the norm of these two normal vectors. All computations used in method 1 are carried out within a small region. Figure 2.5 presents an operation of method 1.
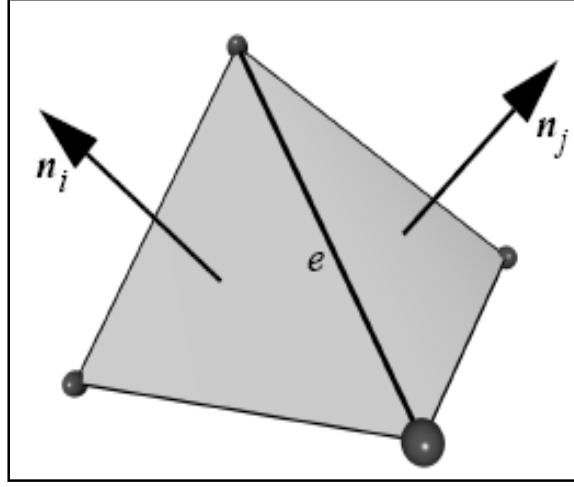
Figure 2.5 Operation of method 1
(Adapted from Hubeli and Gross, 2001)

The operation of method 2 is to extend operation of method 1 using more support to assign an angle value to an edge. The equations used in method 2 to compute an angle value assigned to an edge are defined as:

$$N_i = Average\ Normal\ Vectors\ on\ the\ vertices\ x_i \qquad (2.2)$$

$$N_i = \frac{Sum\ of\ Normal\ Vectors\ of\ the\ triangles\ on\ the\ vertices\ x_i}{Number\ of\ the\ triangles\ on\ the\ vertices\ x_i} \qquad (2.3)$$

$$N_j = Average\ Normal\ Vectors\ on\ the\ vertices\ x_j \qquad (2.4)$$

$$N_j = \frac{Sum\ of\ Normal\ Vectors\ of\ the\ triangles\ on\ the\ vertices\ x_j}{Number\ of\ the\ triangles\ on\ the\ vertices\ x_j} \qquad (2.5)$$

$$A_2(e) = arc\ cos\ (\frac{N_i}{\|N_i\|} \cdot \frac{N_j}{\|N_j\|}) \qquad (2.6)$$

where, N_i and N_j are defined as average normal vectors of the vertices x_i and x_j opposite to the edge e. These average normal vectors are computed using all the normal vectors of the triangles on the vertices x_i and x_j. $A_2(e)$ is an angle value assigned to the edge e, and it is computed using the average normal vectors N_i and N_j. Using the equations of method 2, all computations are carried out in a large region, and the influence of noises is reduced. Figure 2.6 presents an operation of method 2.
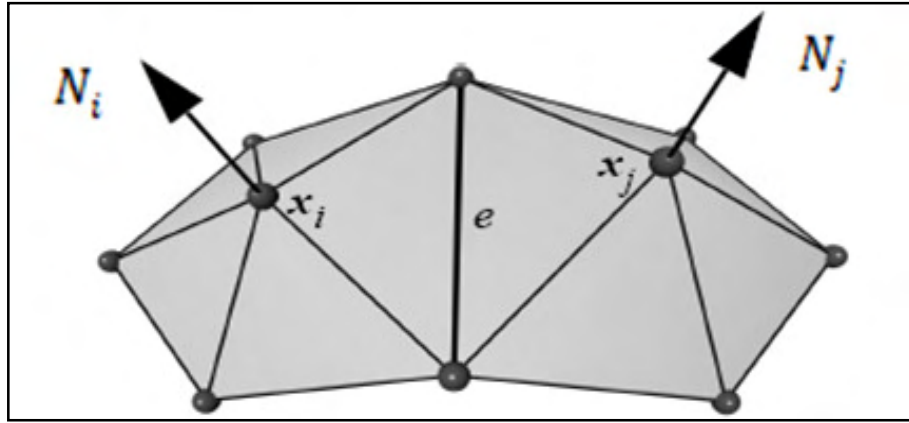
Figure 2.6 Operation of method 2
(Adapted from Hubeli and Gross, 2001)

2.5 Determination of the range of angle values with hypothesis testing

Hypothesis testing is used to determine the range of angle values in which important edges, including bluff edges, are well extracted from the triangle mesh. If an angle value assigned to an edge is higher than angle a° and lower than angle b°, the edge is identified as an important edge. Figure 2.7 illustrates operation of selection of important edges using hypothesis testing.

29
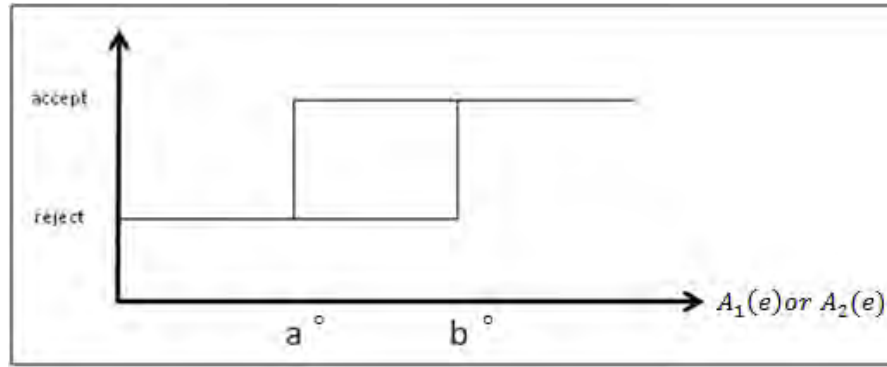
Figure 2.7 Operation of determination of the range of angle values using hypothesis testing

There are two ranges employed by hypothesis testing.

The two ranges are described below:

a) The first range: $25° \leq$ angle values assigned to an edge ($A_1(e)$ and $A_2(e)$) $\leq 85°$

b) The second range: $3° \leq$ angle values assigned to an edge ($A_1(e)$ and $A_2(e)$) $\leq 25°$

If an edge is located at the region where the slope sharply changes, the angle value assigned to the edge normally has a higher value. In general, the edges which compose breaklines have higher angle values, since these edges are located at the region where the slope sharply changes. Blufflines are similar to breaklines; however, the edges which constitute blufflines are not always located at the region where the slope sharply changes. In some bluff regions, the slope smoothly changes at the bluff top or the bluff toe.

There is no standard angle value which bluff edges have. This thesis assumes that the angle value, assigned to the edge located at the bluff top and the bluff toe in most bluff regions of the study area, is higher than 25° and less than 85°, thus, the range, in which important edges including the bluff edges are well extracted, is determined as 25° ~ 85°.

30

This range is defined as the first range. In the bluff region where the bluff edges are not extracted using the first range, this thesis assumes that the bluff region has an extremely smooth slope near the bluff top and the bluff toe. Thus, another alternative range is needed for extraction of the extra bluff edges. This thesis proposes the alternative range is 3º ~ 25º, and the range is defined as the second range. For extraction of the bluff edges, the first range is applied earlier than the second range, since this thesis assumes that most bluff edges located at the bluff top and the bluff toe are extracted using the first range. In the area where the bluff edges are not extracted at the first range, the second range is applied to extract the extra bluff edges.

In the experiment, 85~95% of the bluff edges which compose the bluffline segments are extracted at the first range, and only 5~15% of the bluff edges are extracted at the second range. Figure 2.8 shows an example of the bluff edges extracted using both ranges.
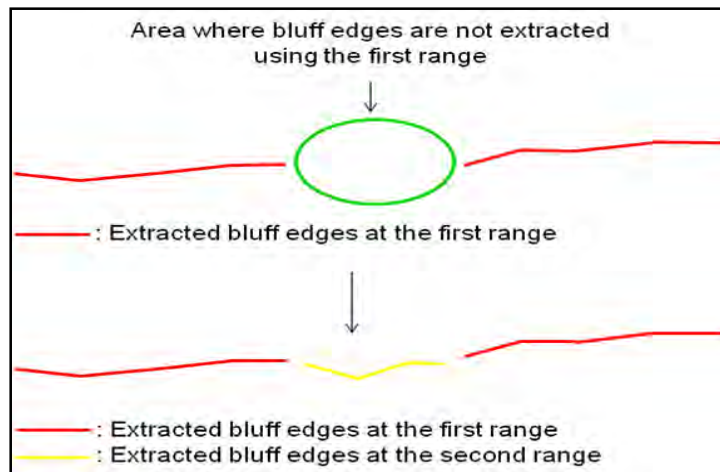
Figure 2.8 Example of bluff edges extracted using both ranges

2.6 Selection of intersection edges

In general, the important edge groups, extracted separately using method 1 and method 2, include the bluff edges. However, both edge groups also include some feature edges which are not suitable for the bluff edges, since the blufflines are not only linear features in bluff region. Thus, utilization of only one method does not provide enough information for extraction of the bluffline segments which consist of the bluff edges.

This thesis proposes to select the intersection edges which are extracted using both methods at the same range for extraction of the bluffline segments. Equation 2.7 shows the operation of selection of the intersection edges.

$$A_i \cap B_i = C_i \tag{2.7}$$

In equation 2.7, i is the index of the range of angle values, A_i is the extracted edge group using method 1 at the i range, B_i is the extracted edge group using method 2 at the i range, and C_i is the intersection edge group extracted using both methods at the i range.

Figure 2.9 shows one simple example of the intersection edges extracted using both methods at the i range.
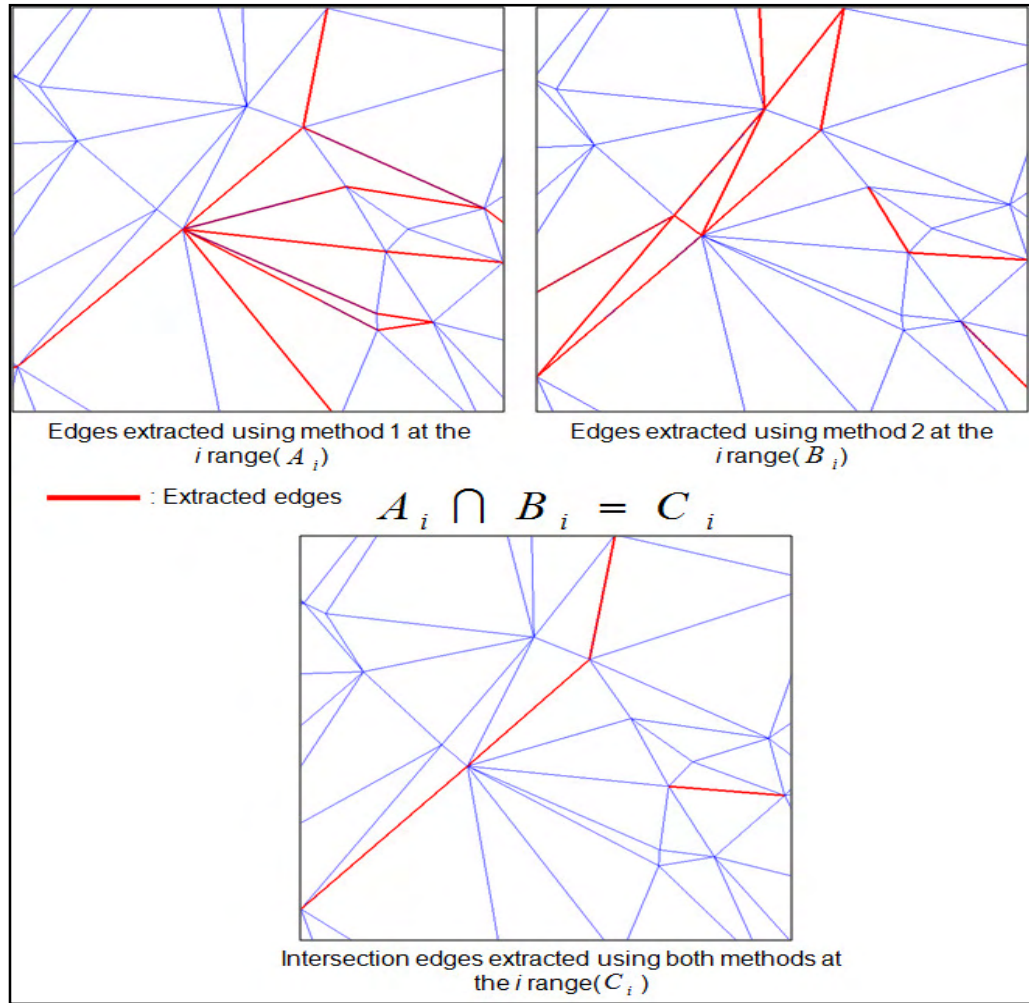
Figure 2.9 Example of the intersection edges

2.7 Elimination of unsuitable edges

The intersection edge group includes the bluff edges which compose the bluffline segments; however, they still include some linear feature edges unsuitable to compose the bluffline segments. The objective of this step is to eliminate the edges, which are not suitable to compose the bluffline segments, as much as possible considering vertical distance, slope and connectivity of an edge. There are two sub-steps included in the step

of elimination of unsuitable edges. In each sub-step, the unsuitable edge groups are defined by using specific characters of the edge, and each sub-step is applied step by step to remove unsuitable edges from the intersection edge group. Each sub-step to define unsuitable edges is explained below.

1) Sub-step 1

In sub-step 1, unsuitable edges are defined by considering vertical distance and slope of each edge. The edge group which is eliminated in sub-step 1 is explained below

    a) The edge with vertical distance higher than 1.0668 m should be eliminated in sub-step 1.

    b) Considering both end points of an edge, the edge with slope larger than 60º should be eliminated in sub-step 1.

In general, the edges located at bluff face and vertical features have high vertical distance and large slope. Hence, the edges with high vertical distance or large slope are considered as the feature edges located vertical features, uplands or bluff face. Considering the height of vertical features and the point density of the LiDAR data, this thesis assumes that the edges with vertical distance higher than 1.0668m or slope larger than 60º are considered as the edges which compose vertical features or the edges located on bluff face, and these edges are eliminated in sub-step 1. Thus, after sub-step 1, the edges with vertical distance smaller than 1.0668m and slope smaller than 60º remain after sub-step 1.

2) Sub-step 2

In sub-step 2, unsuitable edges are defined by considering the edge connectivity. The edge group which is eliminated in sub-step 2 is explained below.

a) The single edge, where both end points are not linked to any other edges, should be eliminated in sub-step 2.

b) The edge, where one of end points is linked to multiple edges and the other end point is not linked to any other edges, should be eliminated in sub-step 2.

Each sub-step is applied step by step in the step of elimination of unsuitable edges. After sub-step 1 is applied to remove the unsuitable edges from the intersection edge group, sub-step 2 is applied to remove the extra unsuitable edges.

After the two sub-steps are applied, most edges which are not suitable to compose the bluffline segments are eliminated. Figure 2.10 displays an example of the process to remove the unsuitable edges from the intersection edge group by successive application of the two sub- steps.
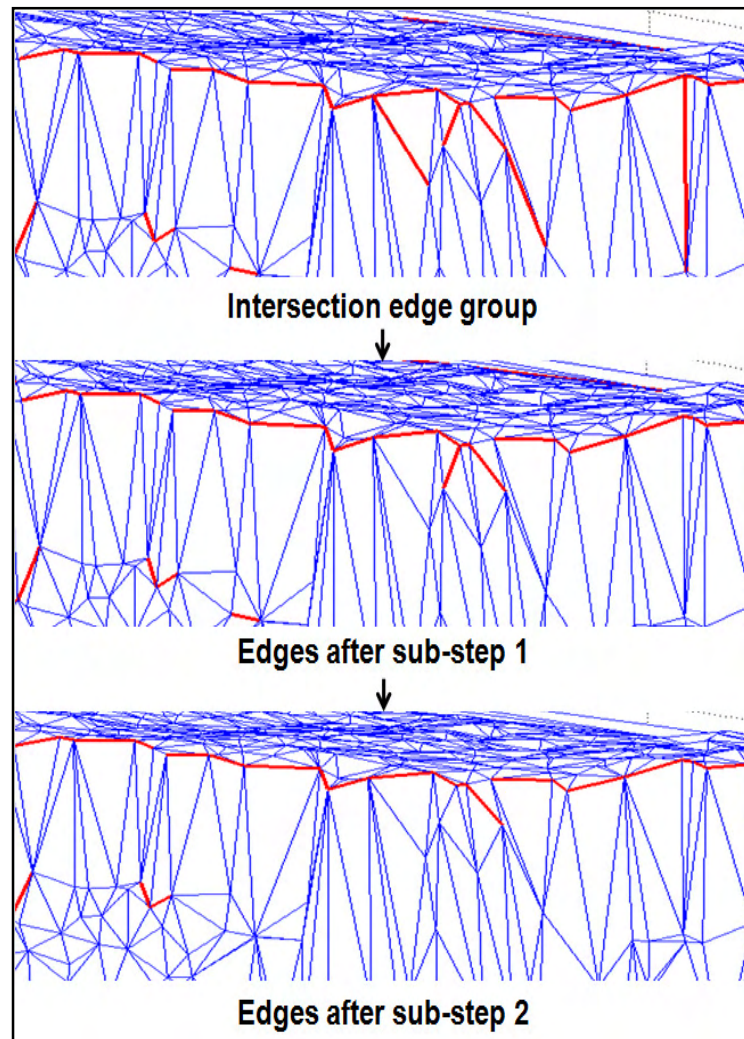
Figure 2.10 Example of the process to remove the unsuitable edges from the intersection edge group

As seen in Figure 2.10, few edges which are not suitable to compose the bluffline segments still remain after the step of elimination of unsuitable edges.

2.8 Extraction of line segments

The objective of this step is to extract the line segments from the remaining edge group. There are two sub-steps which the line segments should satisfy. The line segments would be selected after two sub-steps are applied step by step, and the two sub-steps are explained below.

- Sub-step 1. If two adjacent triangles which share the edge of the remaining edge group do not have any other edges belonging to the remaining edge group, the edge is selected in sub-step 1.

- Sub-step 2. Among the edges selected in sub-step 1, multi-linked edges are defined as line segments.

Figure 2.11 shows an example of the line segments which satisfy the two sub-steps.
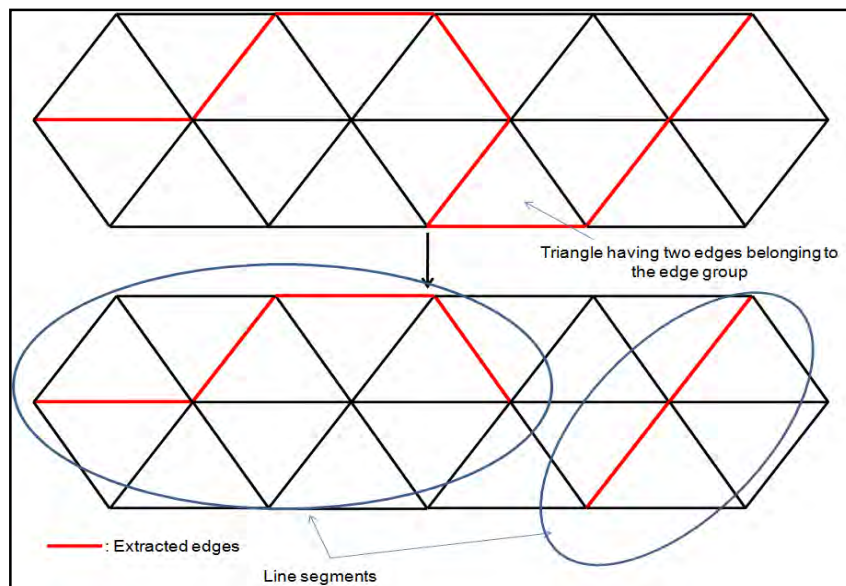
Figure 2.11 Example of the extracted line segments

37

Most line segments extracted in this step are located at the bluff top and the bluff toe, and only few line segments are located on bluff face or uplands. The line segments which are located as the bluff top and the bluff toe are considered as the bluffline segments. Figure 2.12 shows examples of the line segments located at the bluff top and the bluff toe after the step of extraction of line segments.

Line segments located at the bluff top

Line segments located at the bluff toe
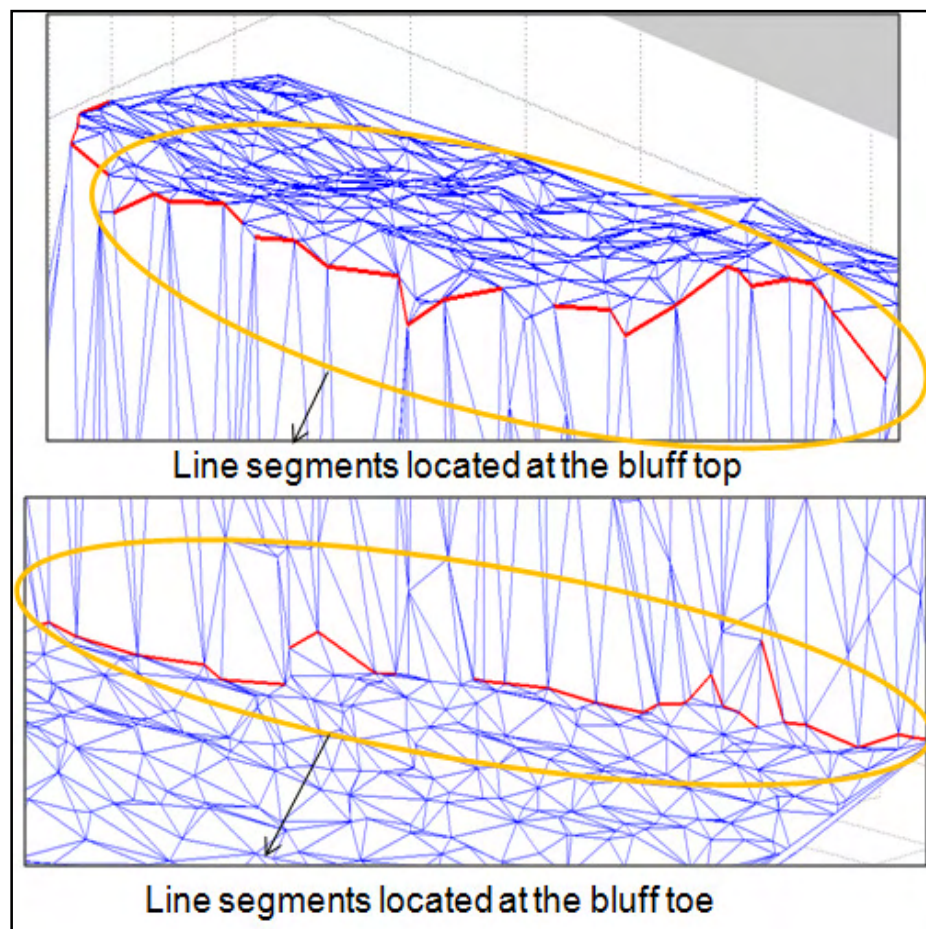
Figure 2.12 Examples of the bluffline segments

In Figure 2.12, there are gaps between the bluffline segments. If the gap is only one triangle edge between the bluffline segments, the edge is also considered as the bluff edge which composes the bluffline segments; however, if the gap is larger than multi-linked edges, a straight line is needed to link between the bluffline segments. In Figure 2.13, a straight line (the green line) is generated in the gap between two bluffline segments for construction of the three dimensional blufflines, and these straight lines are considered as the disconnected bluffline segments. In general, these disconnected bluffline segments are generated in the area where the bluff region has an extremely smooth surface near the bluff top and the bluff toe.

2.9 Linkage of bluffline segments to construct blufflines

With all the bluffline segments located at the bluff top and the bluff toe, one bluffline segment is manually connected to another bluffline segment with the end points of both bluffline segments located nearest horizontally and vertically to each other. After linkage of all the bluffline segments, the bluff toe line and the bluff top line are generated. Figure 2.13 displays an example of linkage of the bluffline segments for construction of the three dimensional blufflines.

Figure 2.14 shows the extracted blufflines using the vector based method. In Figure 2.14, the yellow line is the constructed bluff toe line, and the red line is the constructed bluff top line.
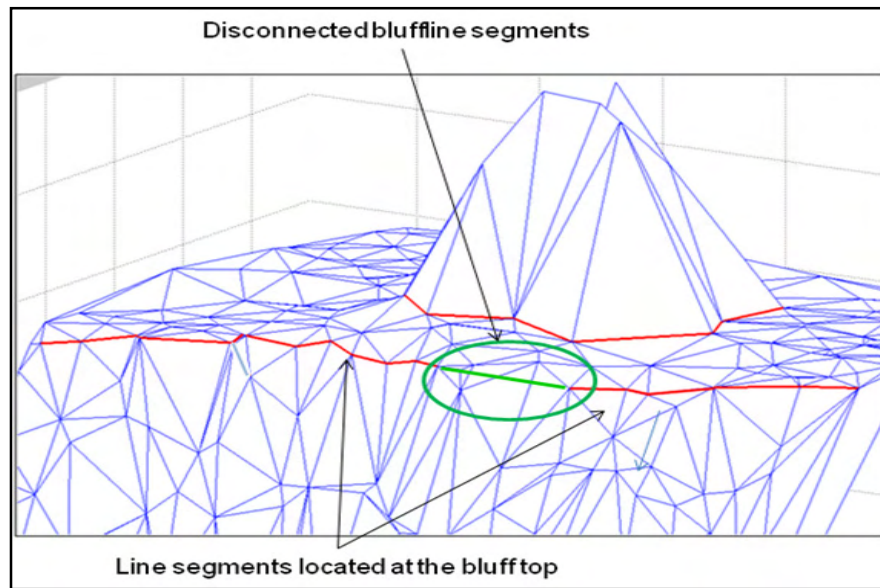
Figure 2.13 Example of linkage of the bluffline segments
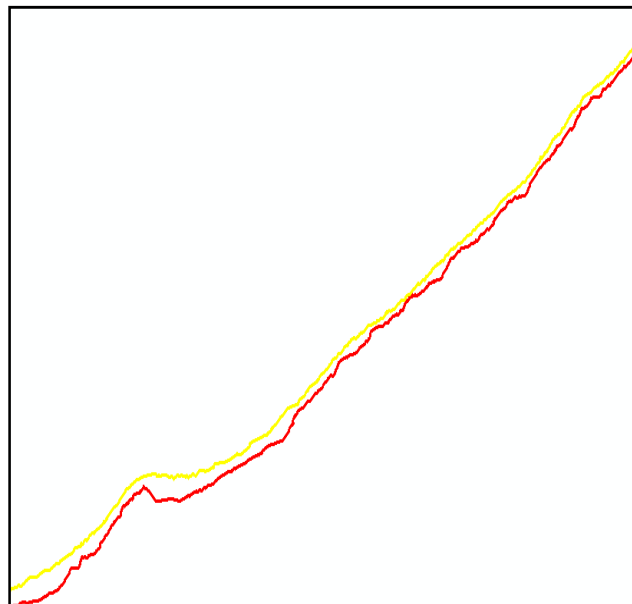
Figure 2.14 Blufflines extracted using the vector based method

CHAPTER 3: DATA PREPARATION AND

IMPLEMENTATION

3.1 Introduction

This chapter discusses the study area, all data sources used in this research and all procedures of implementation for this research.

3.2 Description of study area

The study area for this research is located in Painesville, Ohio, a two kilometer coastal region along the southern coast of Lake Erie. Figure 3.1 shows the aerial view of the study area.

There are several reasons for choosing this area for this research.

1) LiDAR data, historical blufflines and satellite images of this region are available to provide enough information of the region for coastal modeling and analysis.

2) The Division of Geological Survey of the ODNR is interested in this region, identifying it as an area highly vulnerable to severe coastal erosion (Zuzek et al., 2003; Srivastava et al., 2005). The retreat rate in this area is 1.04 m/year from 1973 to 2000 (Liu et al., 2009). Such high retreat rate is caused by the serious coastal erosion. The significant coastal erosion has caused property loss and damage to coastal protection structures in the study area (Liu et al., 2009). In this area, there is vegetation near the bluff top.
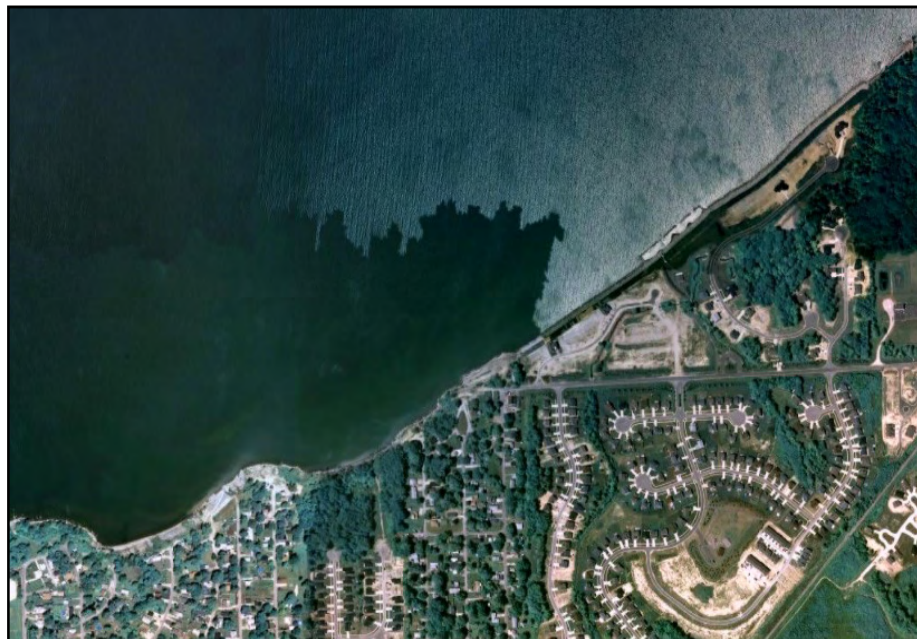
Figure 3.1 The aerial view of the study area, Lake Erie, Painesville, Ohio (Captured from Google Earth^{TM} , last date accessed: 03 August 2009)

3.3 Description of data set

This section discusses the spatial data set used in this research. The LiDAR data is used as a main source for this research. The aerial orthoimages are used as reference surfaces for determination of the ground truths.

3.3.1 Description of the LiDAR data

The LiDAR data used in this thesis was acquired in December, 1998 using a LiDAR sensor of ATM at a speed of 60 meters per second. This LiDAR data was collected by the NOAA Costal Center Service for academic research. The vertical accuracy of this LiDAR data is 15 cm, and the horizontal accuracy of this LiDAR data is 0.8 m (http://maps.csc.noaa.gov/TCM/viewdesc.jsp?pc=2&mid=7). The horizontal datum of this LiDAR data is North American Datum 1983 (NAD83), and the vertical datum of this LiDAR data is International Great Lakes Datum 1985 (IGLD85). The nominal ground spacing of this LiDAR data is 3 m. Figure 3.2 shows the LiDAR data used in this research.

Figure 3.2 The LiDAR data used in this research

3.3.2 Description of the aerial orthoimage data

In this research, the aerial orthoimages were used as reference surfaces. The aerial orthoimages were acquired in April, 2000. The check points, used for measurement of accuracy of the extracted blufflines using the slope based method and the vector based method, are obtained from the aerial orthoimages. The aerial orthoimages were georeferenced using the State Plane Coordinate System (Ohio North) based on the horizontal datum NAD83, and the ground resolution of the aerial orthoimages is 0.15 m. Figure 3.3 shows the aerial orthoimages used as reference surfaces in this research.

Figure 3.3 The aerial orthoimages used in this research

3.4 Implementation

This section discusses all implementations of this research with the acquired LiDAR data.

A commercial GIS (Geographic Information System) tool (ArcMap Version 9.3) and

MATLAB Version 7.0.1 are used for implementation of this research. Figure 3.4 presents

the flow diagram showing the process of implementation of all the methods in this

research.
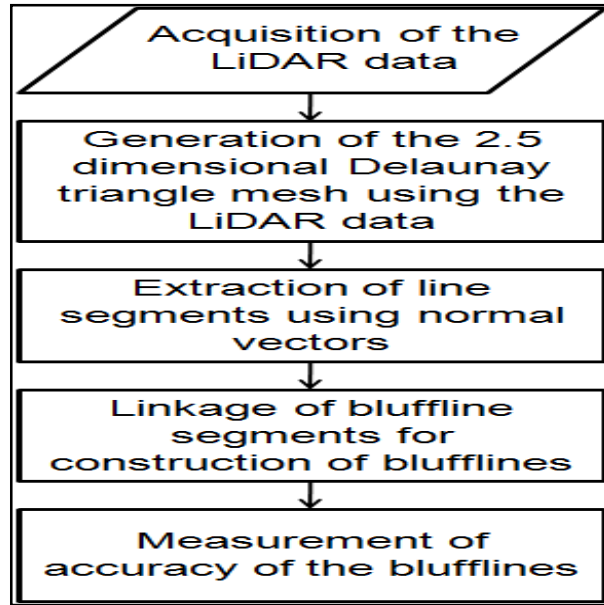
Figure 3.4 Flow diagram showing the process of all implementations
in this research

The LiDAR data of the study area can be obtained in the website of the NOAA coastal

service center (http://csc-s-maps-q.csc.noaa.gov/TCM/). After determination of interest

area, the horizontal datum and the vertical datum, the LiDAR data can be obtained. The

obtained LiDAR data is imported to MATLAB, and all computations used in the vector

based method with the imported LiDAR data are carried out using MATLAB. MATLAB

is a mathematical computing language developed and maintained by MathWorks.

Multiple functions, such as matrix manipulations, data plotting, mathematical

computation, etc. are available in MATLAB. MATLAB also provides the function for

generation of the Delaunay triangle mesh using a set of points of the LiDAR data and its

visualization environment. Computation of normal vector of each triangle, computation

of norm of each normal vector, and computation of an angle value defined by two normal

vectors are available in MATLAB. After extraction of all the bluffline segments using all computations with MATLAB, linkage of all the bluffline segments to generate the three dimensional blufflines are implemented in Arc Map, one of the components of ESRI's ArcGIS. After construction of the three dimensional blufflines, measurement of accuracy of the blufflines is also carried out in ArcMap.

The total length of each bluffline is approximately 2 km. The extracted blufflines using the vector based method consist of the bluffline segments, which consist of the bluff edges, and the disconnected bluffline segments, which are the generated straight lines, located between the extracted bluffline segments. Table 3.1 illustrates information of the disconnected bluffline segments, and Table 3.2 illustrates information of the extracted bluff edges which compose the bluffline segments.

Blufflines	Total length of the disconnected bluffline segments	Number of the disconnected bluffline segments
Bluff Top	729.899 m	76
Bluff Toe	569.053 m	71

Table 3.1 Information of the disconnected bluffline segments

Blufflines	Total length of the extracted bluff edges	Number of the extracted bluff edges
Bluff Top	1265.757 m	645
Bluff Toe	1424.317 m	802

Table 3.2 Information of the extracted bluff edges

47

CHAPTER 4: RESULT AND ANALYSIS

4.1 Determination of the check points

This section discusses determination of the check points used for measurement of accuracy of the extracted blufflines using both methods. In Figure 4.1, the green lines are the manually digitized blufflines from the aerial orthoimages, the green points are the check points of each bluff top line and each bluff toe line, and the yellow lines are the transects. All the check points of the bluff toe and the bluff top are determined at the intersection of each transect with the digitized bluff top line and the digitized bluff toe line (Liu et al., 2009). The average distance between each check point is 30 m, since the average distance between the transects is 30 m. The X, Y coordinates of these check points are obtained from the aerial orthoimages, and the Z coordinates of them are obtained from the LiDAR data (Liu et al., 2009).

In this research, 53 check points are used for measurement of accuracy of the bluff top lines, and 56 check points are used for measurement of accuracy of the bluff toe lines. 3 check points of the bluff top are removed due to thick vegetation located near the bluff top.
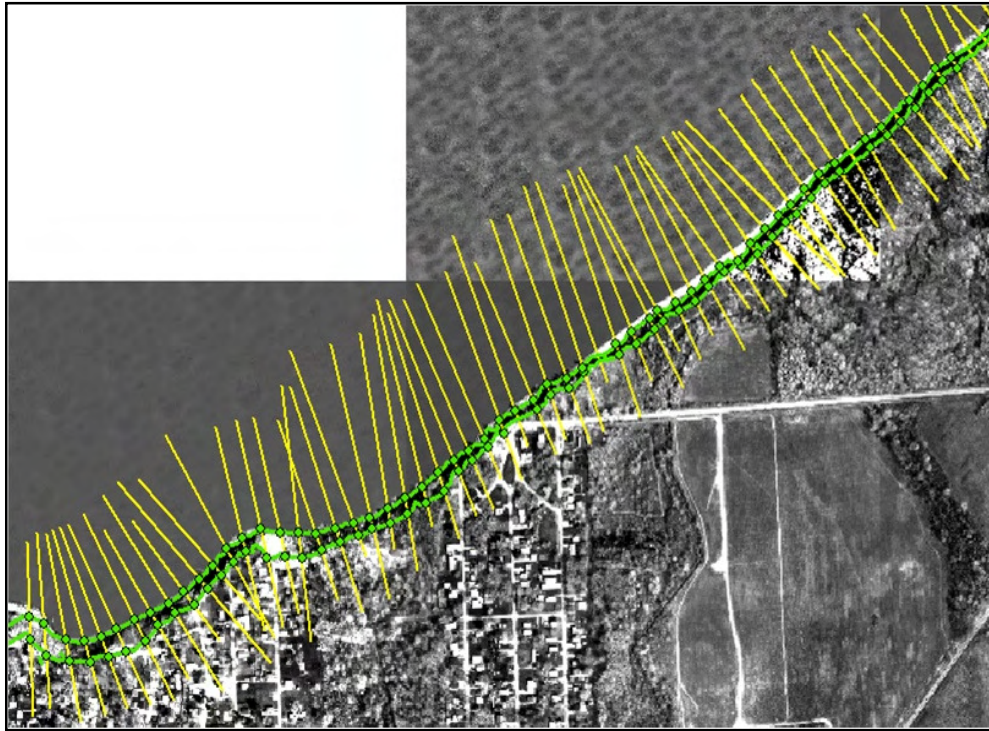
Figure 4.1 Check points determined at the intersection of transects with the manually digitized blufflines

Figure 4.2 shows all three blufflines including the manually digitized blufflines, the extracted blufflines using the vector based method and the extracted blufflines using the slope based method in the whole study area. In Figure 4.2, the whole area is divided into three sub-regions. Figure 4.3 shows all three blufflines in sub-region 1 of the study area, Figure 4.4 shows all three blufflines in sub-region 2 of the study area, and Figure 4.5 shows all three blufflines in sub-region 3 of the study area.
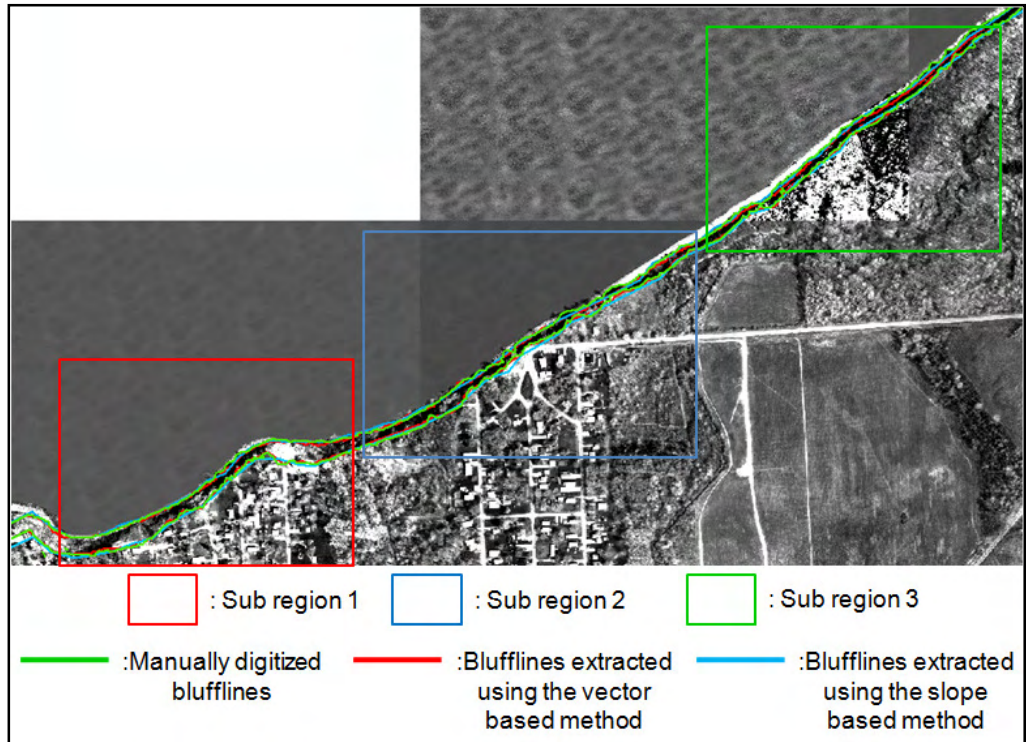
Figure 4.2 All three blufflines in the whole study area
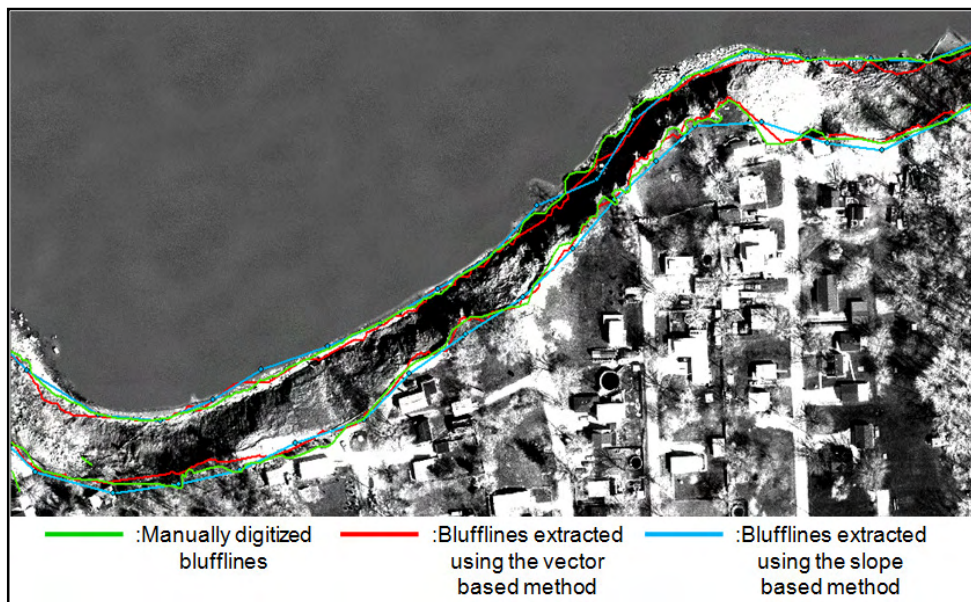
Figure 4.3 All three blufflines in sub-region 1 of the study area
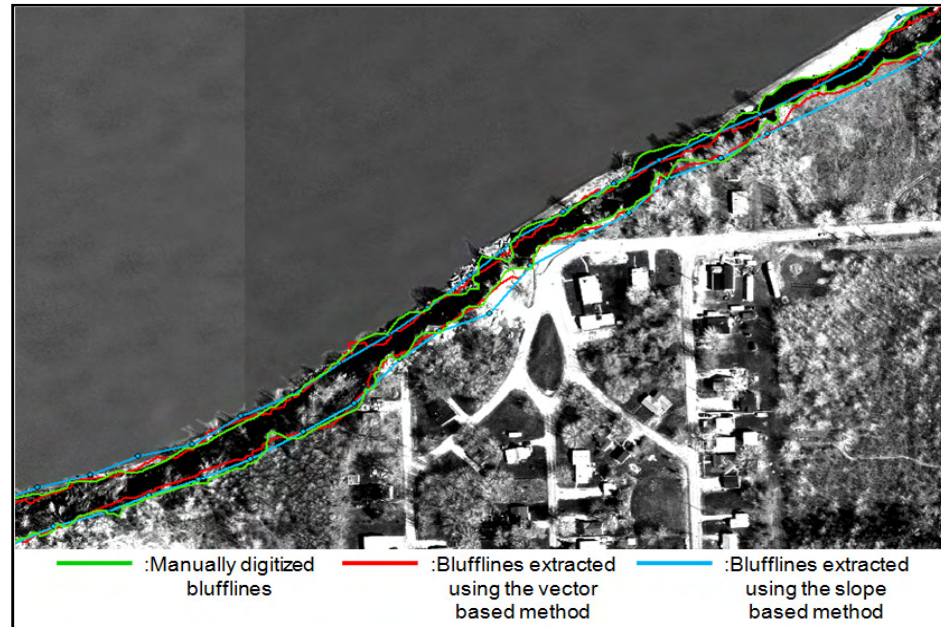
Figure 4.4 All three blufflines in sub-region 2 of the study area
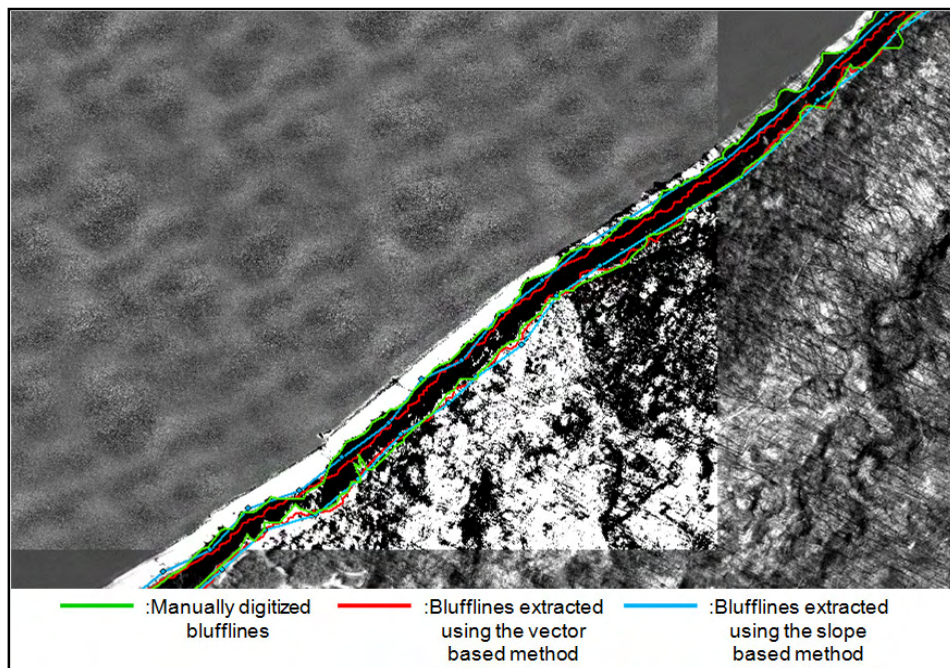
Figure 4.5 All three blufflines in sub-region 3 of the study area

4.2 Methods for measurement of accuracy of blufflines

The method for measurement of horizontal accuracy of the extracted blufflines is to measure the shortest horizontal distance from each check point to the bluff top or toe point on the blufflines, and the method for measurement of vertical accuracy of the extracted blufflines is to measure the vertical distance from each check point to the same bluff top or toe point on the blufflines. All the bluff top and toe points extracted using the slope based method and the check points are determined along the transects (Liu et al., 2009). Hence, the shortest horizontal distance from each check point to the bluff top or toe point on the blufflines is the horizontal distance from each check point to the bluff top or toe point along the transect. The vertical accuracy of the extracted blufflines is implemented by measurement of the vertical distance from each check point to the same bluff top or toe point.

However, the horizontal distance from each check point to the bluff top or toe point on the extracted blufflines, using the vector based method, along the transect is not the shortest horizontal distance, since, using the vector based method, the bluffline segments are not generated along the transect. Figure 4.6 shows an example of locations of a check point, a transect, the extracted bluffline using the vector based method. In Figure 4.6, the horizontal distance from the check point to the bluff top or toe point on the bluffline with the transect is not the shortest horizontal distance from each check point to the blufflines.

For measurement of accuracy of the extracted blufflines using the vector based method, the point, which is located nearest the each check point in horizontal direction, is obtained on the blufflines. This point is defined as the identified bluff top or toe point on

the extracted blufflines using the vector based method. The horizontal distance from each check point to the identified bluff top or toe point on the blufflines is the shortest horizontal distance from each check point to the extracted blufflines using the vector based method.

Thus, measurement of horizontal accuracy of the extracted blufflines using the vector based method is implemented by measurement of the horizontal distance from each check point to the identified bluff top or toe point on the blufflines, and measurement of vertical accuracy of the blufflines is implemented by measurement of the vertical distance from each check point to the same bluff top or toe point on the blufflines. The X, Y coordinates of these identified bluff top and toe points are obtained from the aerial orthoimages, and the Z coordinates of them are obtained from the LiDAR data.

Figure 4.7 shows the method for accuracy of the blufflines extracted using the vector based method. In Figure 4.7, the horizontal distance (r) from the identified bluff top or toe point on the blufflines to each check point and the vertical distance (dz) from the same bluff top or toe point on the blufflines to each check point are measured for accuracy of the extracted blufflines using the vector based method.
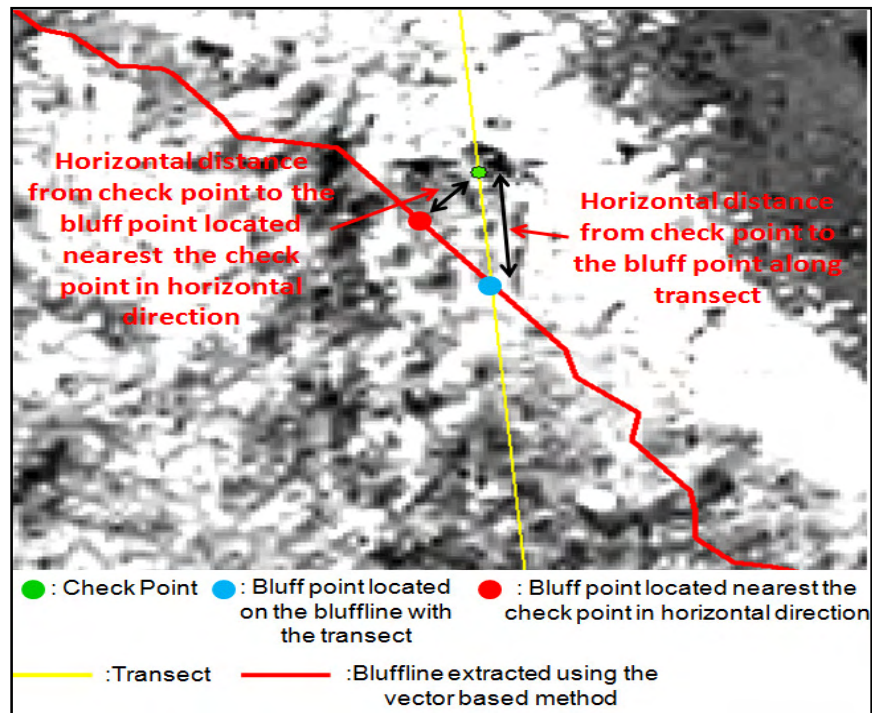
Figure 4.6 Locations of a check point, a transect, the extracted bluffline using the vector based method
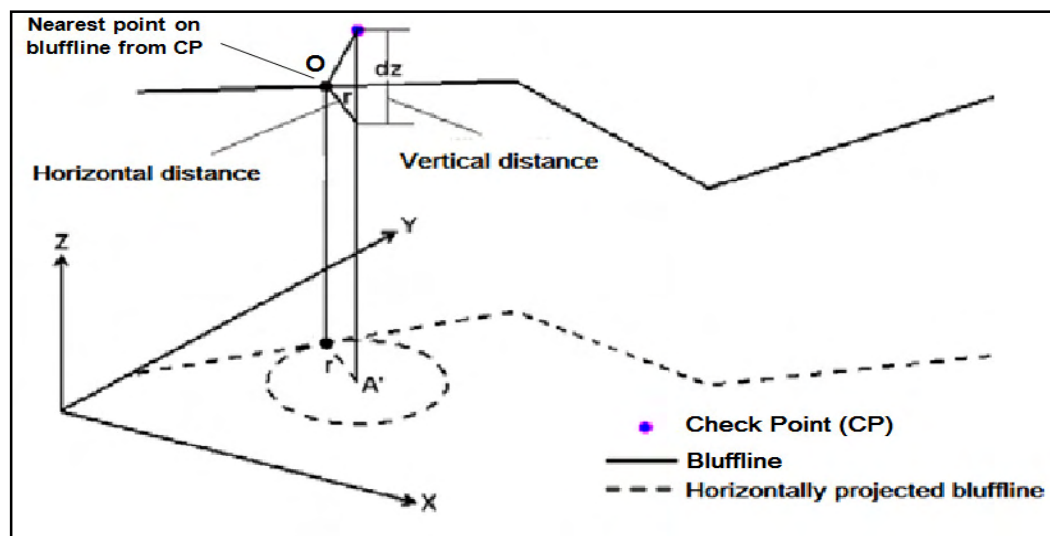
Figure 4.7 Method for measurement of accuracy of the extracted blufflines using the vector based method

4.3 Results and analysis

This section discusses the measurement results. Measurements of accuracy of the extracted blufflines using both methods are carried out by using the same check points. The method for measurement of accuracy of the extracted blufflines is to measure the absolute horizontal distance and the absolute vertical distance from each check point to the identified bluff top or toe point.

This section also discusses analysis of the measurement results. All the bluff top and toe points on the extracted blufflines have the horizontal and vertical measurement results with each check point. Analysis is implemented with the bluff top and toe points which have the outliers. In this research, the outliers are considered as the values which are higher than the value of $3 \cdot \sigma$(standard deviation) $+ \mu$(average) or which are similar to the values of $3 \cdot \sigma + \mu$.

1) Bluff Top

Table 4.1 illustrates the measurement results of horizontal accuracy of the two bluff top lines, and Figure 4.8 shows the measurement results of the absolute horizontal distance from the identified bluff top point to each check point.

Bluff Top	Maximum distance (meter)	Minimum distance (meter)	Average distance (meter)	Standard Deviation (meter)
Bluff top extracted using the slope based method	8.264	0.155	2.201	1.707
Bluff top extracted using the vector based method	6.553	0.035	1.838	1.507

Table 4.1 The measurement results of horizontal accuracy of the two bluff top lines
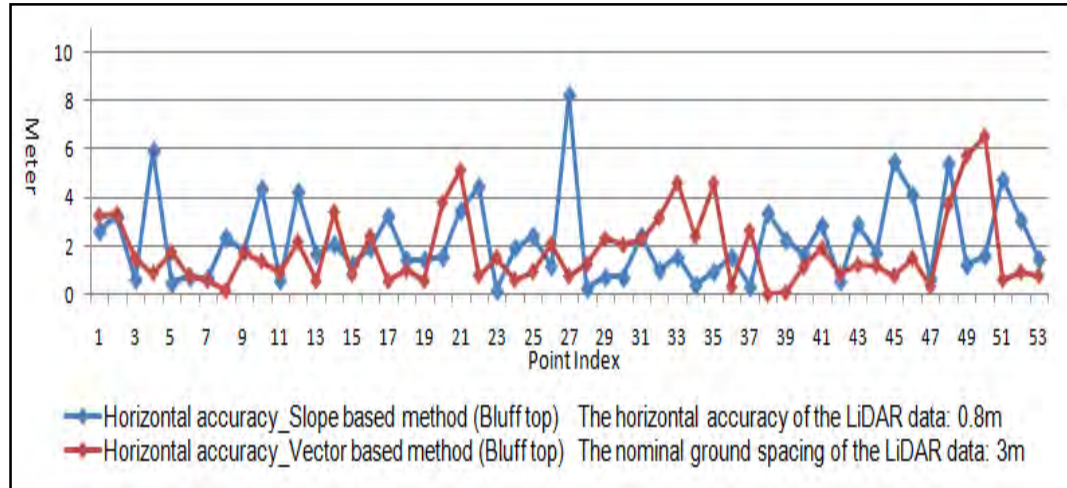
Figure 4.8 The measurement results of the absolute horizontal distance from the identified bluff top point to each check point

56

Reasons for the horizontal outliers of the identified bluff top points using the slope based method are explained below.

1) The maximum slope along the slope profile is extremely larger than any other slope values or slope values of the points on the bluff top are lower than the slope constraint (The outlier with check point 4).

2) The minimum slope along the slope profile is not lower than -0.4 (The outlier with check point 27).

Reasons for the horizontal outliers of the identified bluff top points using the vector based method are explained below.

1) The identified bluff top point is located on the disconnected bluffline segments (The outlier with check point 49).

2) The check point is located on a smooth surface near the bluff top (The outlier with check point 50).

Figure 4.9 shows the aerial view and the result of the identified bluff top point using the slope based method with check point 4.

: Check Point   : The identified bluff top point using the slope based method   : The identified bluff top point using the vector based method

——— :Manually digitized blufflines   ——— :Blufflines extracted using the slope based method   ——— :Blufflines extracted using the vector based method

(a) Aerial view

: Bluff top   : Multiple bluff top candidates

: Points on the elevation profile

(b) Location of the identified bluff top point in the elevation profile

$BSlope_{max}$ / 4 (SC)

Slope values of the points on the bluff top

(c) Slope profile

Figure 4.9 The aerial view and the result of the extracted bluff top point using the slope based method with check point 4

In Figure 4.9(c), slope values of the points on the bluff top are less than the SC ($BSlope_{max}/4$); hence, the points on the bluff top cannot be selected as the multiple bluff

top candidates. It causes the identified bluff top point to have a horizontal and vertical outlier with check point 4.

Figure 4.10 shows the aerial view and the result of the identified bluff top point using the slope based method with check point 27.

(a) Aerial view

(b) Location of the identified bluff top point in the elevation profile

(c) Slope profile
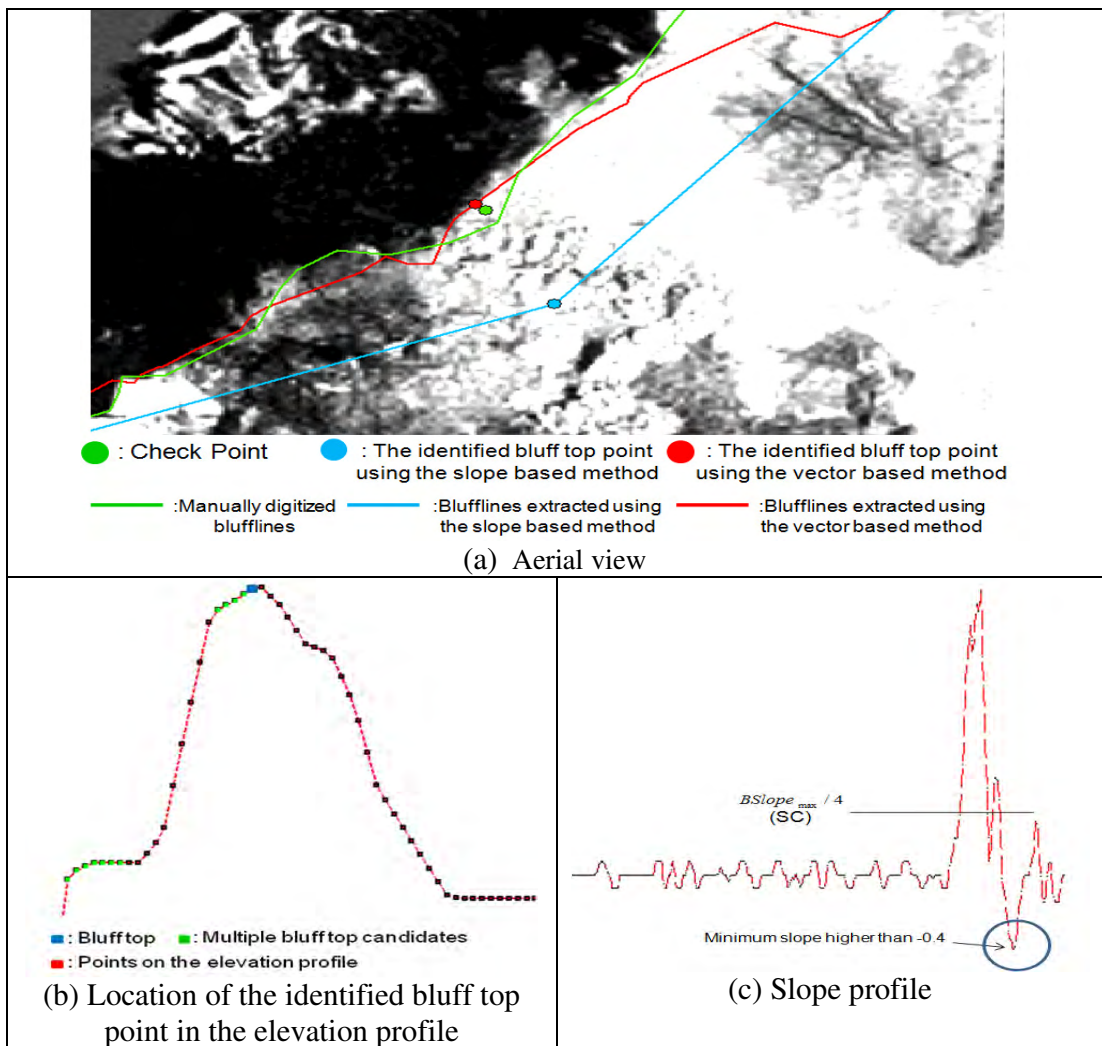
Figure 4.10 The aerial view and the result of the identified bluff top point using the slope based method with check point 27

The slope based method has the following principle to detect points which constitute vertical features along the slope profile: If the minimum slope ($BSlope_{min}$) along the slope profile is below -0.4, all of the points which are below the threshold $BSlope_{min}/2$ are considered as candidates of vertical features (Liu et al., 2009).

Using the slope based method, detection of the bluff top point is implemented after all vertical feature points are detected and removed. However, if the $BSlope_{min}$ is not lower than -0.4, the vertical feature points cannot be detected and removed using the above principle. In Figure 4.10(c), the $BSlope_{min}$ along the slope profile is higher than -0.4, thus the vertical feature points are not removed, and it causes the vertical feature points to remain in the elevation profile. In Figure 4.10(c), some of the vertical feature points have higher slope values than the SC ($BSlope_{max}/4$), and they are selected as the multiple bluff top candidates. Since the point with the highest elevation among the multiple bluff top candidates is selected as the bluff top point, the identified bluff top point is located on the vertical feature. It causes the identified bluff top point to have a horizontal and vertical outlier with check point 27.

Figure 4.11 shows the aerial view and the result of the identified bluff top points using the vector based method with check points 49 and 50.

(a) Aerial view

- ● : Check Point
- ● : The identified bluff top point using the slope based method
- ● : The identified bluff top point using the vector based method
- —— :Manually digitized blufflines
- —— :Blufflines extracted using the slope based method
- —— :Blufflines extracted using the vector based method

- ● : Check Points
- ● : The identified bluff top points
- —— : Disconnected bluffline segments

(b) Location of the bluff top points in the 2.5 dimensional Delaunay triangle mesh

Figure 4.11 The aerial view and the result of the identified bluff top points using the vector based method with check points 49 and 50

61

In Figure 4.11(a), the bluff region has a smooth surface near the bluff top, and the check points are identified on a smooth surface near the bluff top; hence, the check points are far from the sharp front of the bluff top in horizontal direction. Using the vector based method, the bluffline segments are located at the sharp front of the bluff top or the bluff toe in most bluff region of the study area. Thus, the identified bluff top point using the vector based method has a horizontal outlier with check point 50, since the identified bluff top point is located at sharp front of the bluff top and the check point is located on a smooth surface near the bluff top.

In addition, the identified bluff top point 49 is located on the disconnected bluffline segments. Since the disconnected bluffline segments are not the extracted line segments using the vector based method, the identified bluff top or toe point located on the disconnected line segments generally have a horizontal outlier or the vertical outlier. Thus, the identified bluff top point has a horizontal outlier with check point 49.

Table 4.2 illustrates the measurement results of vertical accuracy of the two bluff top lines, and Figure 4.12 shows the measurement results of the absolute vertical distance from the identified bluff top point to each check point.

Bluff Top	Maximum distance (meter)	Minimum distance (meter)	Average distance (meter)	Standard Deviation (meter)
Bluff top extracted using the slope based method	2.662	0.001	0.617	0.743
Bluff top extracted using the vector based method	2.542	0.012	0.492	0.567

Table 4.2 The measurement results of vertical accuracy of the two bluff top lines
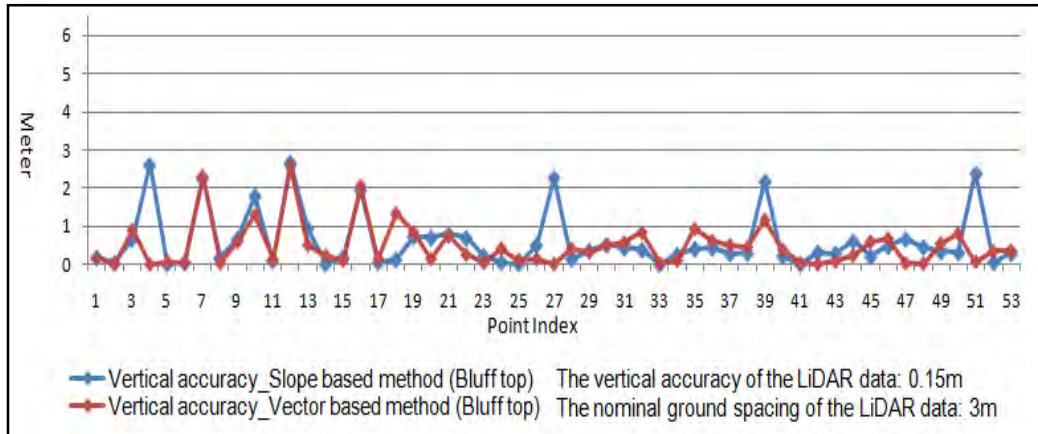
Figure 4.12 The measurement results of the absolute vertical distance from the identified bluff top point to each check point

Reasons for the vertical outliers of the identified bluff top points using both methods are explained below.

1) A lower point density of the LiDAR data at some positions can cause a lower resolution DSM at those positions (The outlier with check point 7).

2) Considering that the LiDAR data and the aerial orthoimages were not taken at the same time, we assume that there were topographic changes during the time period at some positions (The outlier with check point 12).

Figure 4.13 shows the aerial view and the results of the identified bluff top points using both methods with check point 7.

(a) Aerial view

- 🟢 : Check Point
- 🔵 : The identified bluff top point using the slope based method
- 🔴 : The identified bluff top point using the vector based method
- ── :Manually digitized blufflines
- ── :Blufflines extracted using the slope based method
- ── :Blufflines extracted using the vector based method
- 🟡 : LiDAR Points

- 🟦 : Bluff top
- 🟩 : Multiple bluff top candidates
- 🟥 : Points on the elevation profile

(b) Location of the identified bluff top point in the elevation profile

Bluffline segments

- 🟢 : Check Point
- 🔴 : The identified bluff top point using the vector based method

(c) Location of the identified bluff top point in the 2.5 dimensional Delaunay triangle mesh

Figure 4.13 The aerial view and the result of the identified bluff top points using both methods with check point 7

64

Figure 4.13(b) and (c) shows that the identified bluff top points using both methods have a similar horizontal location and vertical location, and they are located on the bluff top. However, Figure 4.13(a) shows that the LiDAR data das has a lower point density in the area. In general, the lower point density of the LiDAR data at some positions causes a lower resolution DSM at those positions. Figure 4.14 shows that, based on the LiDAR DSM, check point 7 has a different elevation value from the identified bluff top points due to the lower point density of the LiDAR data at the position. Since the Z coordinates of the check points are obtained from the LiDAR DSM, the check point has a different elevation value from the identified bluff top points at the position.
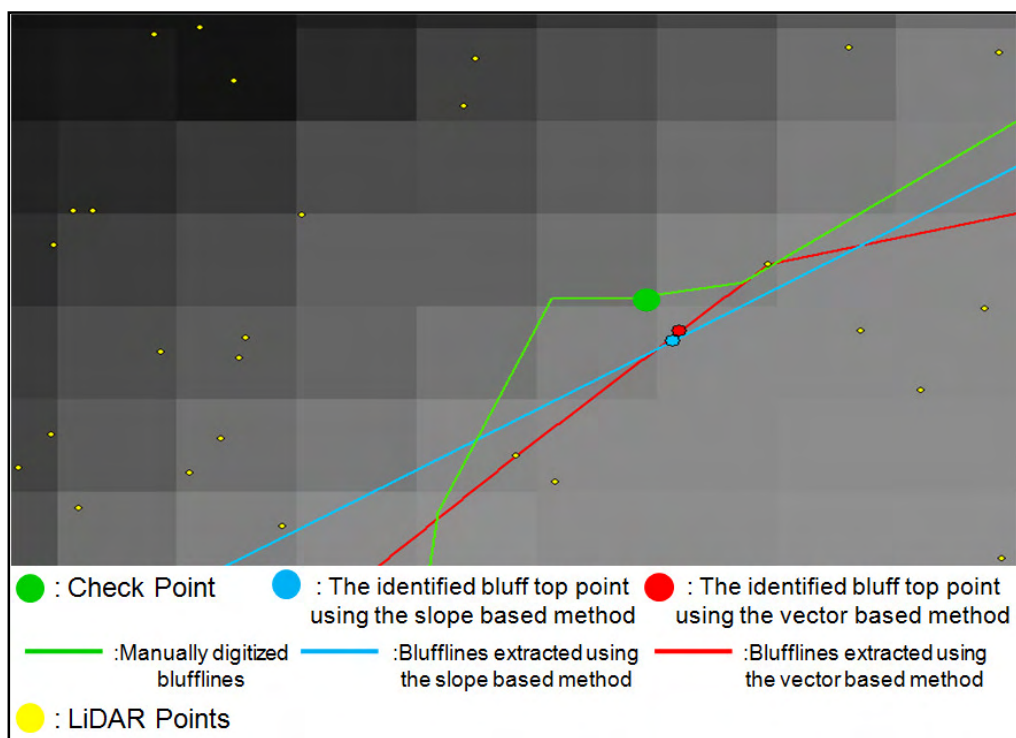
Figure 4.14 Locations of check point 7, the identified bluff top points based on the LiDAR DSM

Figure 4.15 shows the aerial view and the result of the identified bluff top points using both methods with check point 12.

(a) Aerial view

(b) Location of the identified bluff top point in the elevation profile

(c) Location of the identified bluff top point in the 2.5 dimensional Delaunay triangle mesh
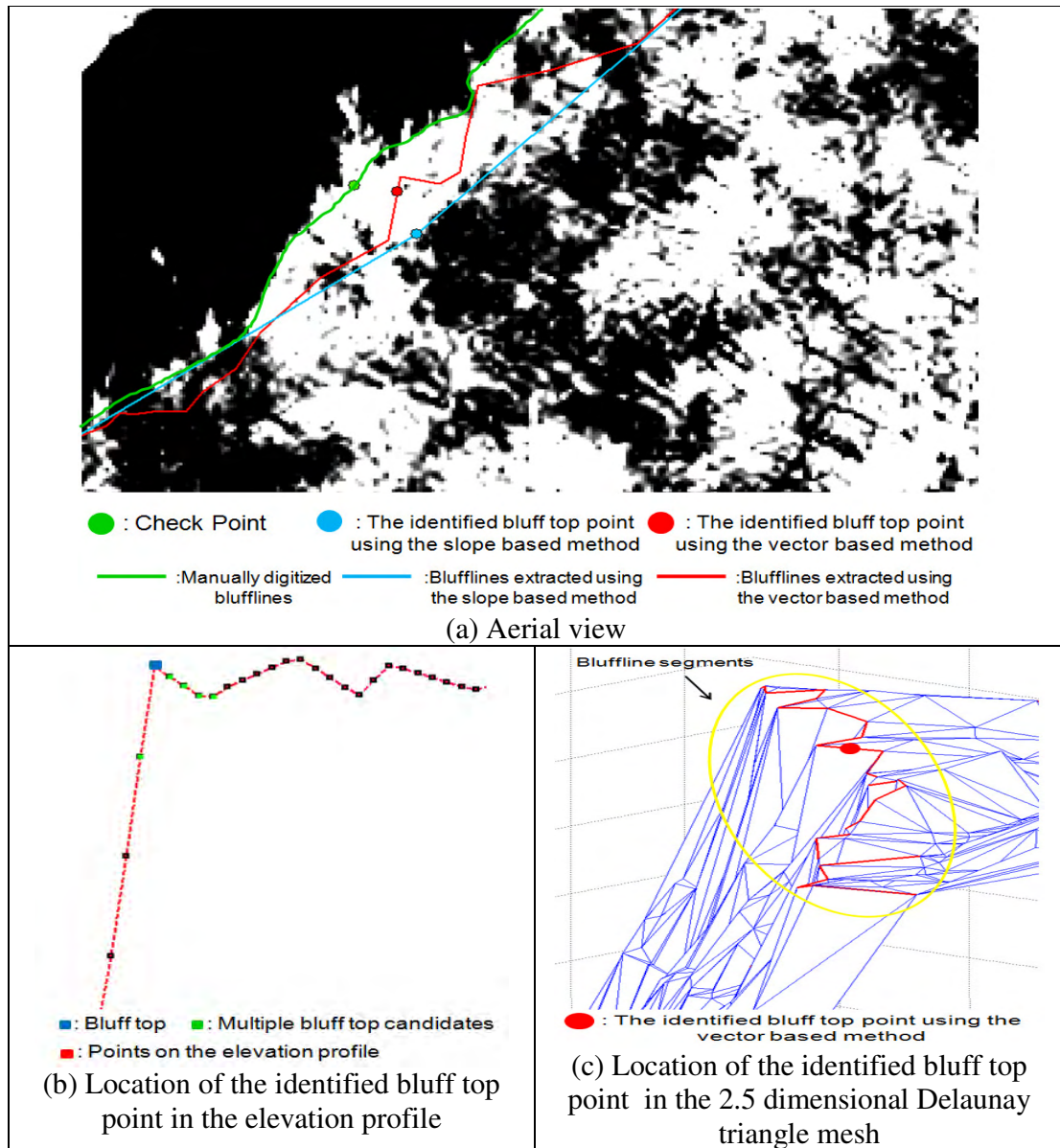
Figure 4.15 The aerial view and the result of the identified bluff top points using both methods with check point 12

Figure 4.15(a) shows that, in the aerial orthoimages, there is a vertical feature between the check point and the identified bluff top points using both methods; however, Figure 4.15(b) and (c) shows that there is no vertical feature near the bluff top in the elevation profile and in the 2.5 dimensional Delaunay triangle mesh. In Figure 4.15, the identified bluff top points using both methods have a similar horizontal and vertical location, and they are located on the bluff top. Thus, we assume that there were topographic changes at the position during the time period when the LiDAR and the aerial orthoimages were taken.

2) Bluff Toe

Table 4.3 illustrates the measurement results of horizontal accuracy of the two bluff toe lines, and Figure 4.16 shows the measurement results of the absolute horizontal distance from the identified bluff toe point to each check point.

Bluff Toe	Maximum distance (meter)	Minimum distance (meter)	Average distance (meter)	Standard Deviation (meter)
Bluff toe extracted using the slope based method	9.943	0.051	2.666	2.189
Bluff toe extracted using the vector based method	9.063	0.029	2.608	2.013

Table 4.3 The measurement results of horizontal accuracy of the two bluff toe lines

Figure 4.16 The measurement results of the absolute horizontal distance from the identified bluff toe point to each check point

Reasons for the horizontal outliers of the identified bluff top points using the slope based method are explained below.

1) The maximum slope along the slope profile is extremely larger than any other slope values (The outlier with check point 22).

2) Due to tidal fluctuation near the shore, some LiDAR points on water have a lower elevation than the water surface. Since the transect is generated near these LiDAR points, some interpolated points, in the reversed elevation profile, located on the water surface have higher slope values than the slope constraint (The outlier with check point 36).

3) The check point is located on a smooth surface near the bluff toe (The outlier with check point 25).

Reason for the horizontal outliers of the identified bluff top points using the vector based method is explained below.

1) The check points are located on smooth surfaces near the bluff toe (The outliers with check points 2, 6, 13, 25).

Figure 4.17 shows the aerial view and the result of the identified bluff toe point using the slope based method with check point 22.

(a) Aerial view

(b) Location of the identified bluff toe point in the elevation profile
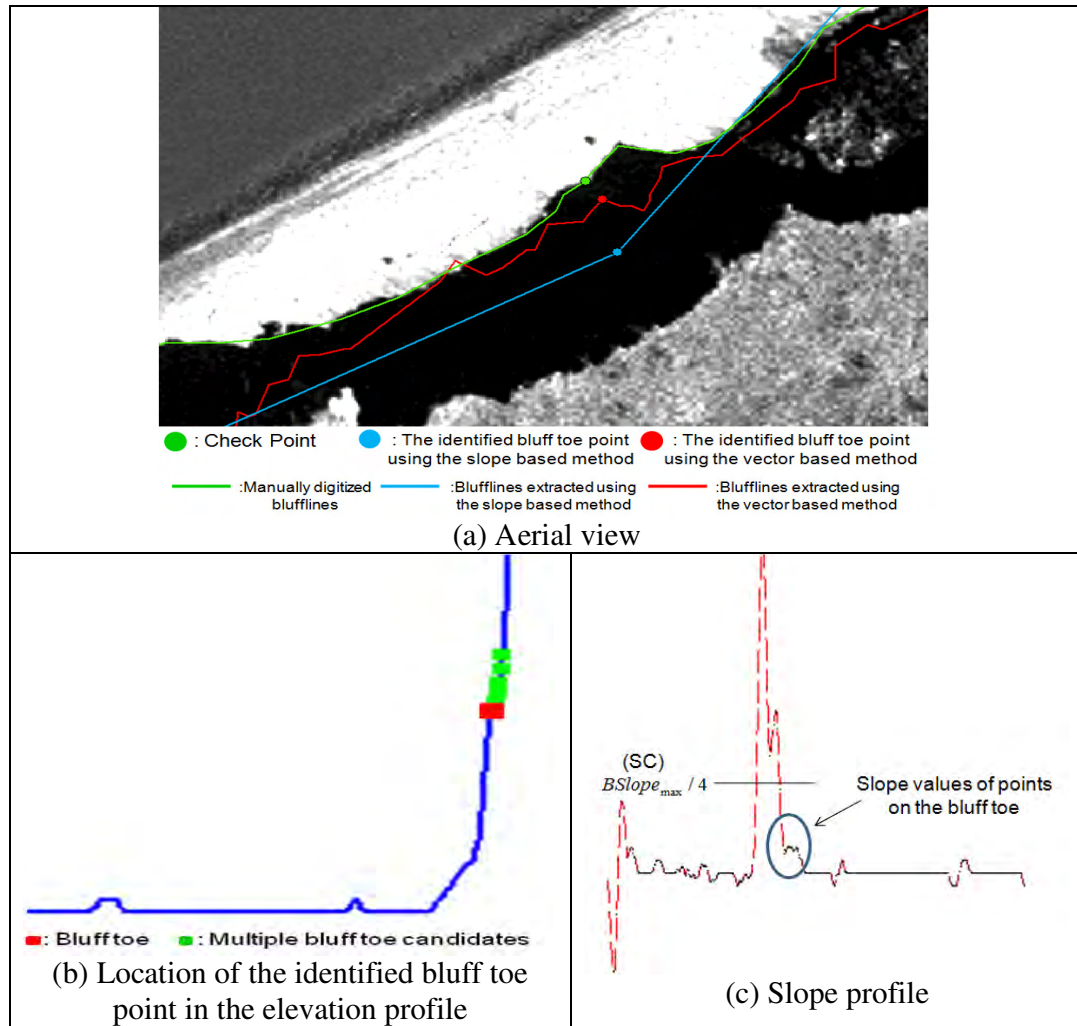
(c) Slope profile

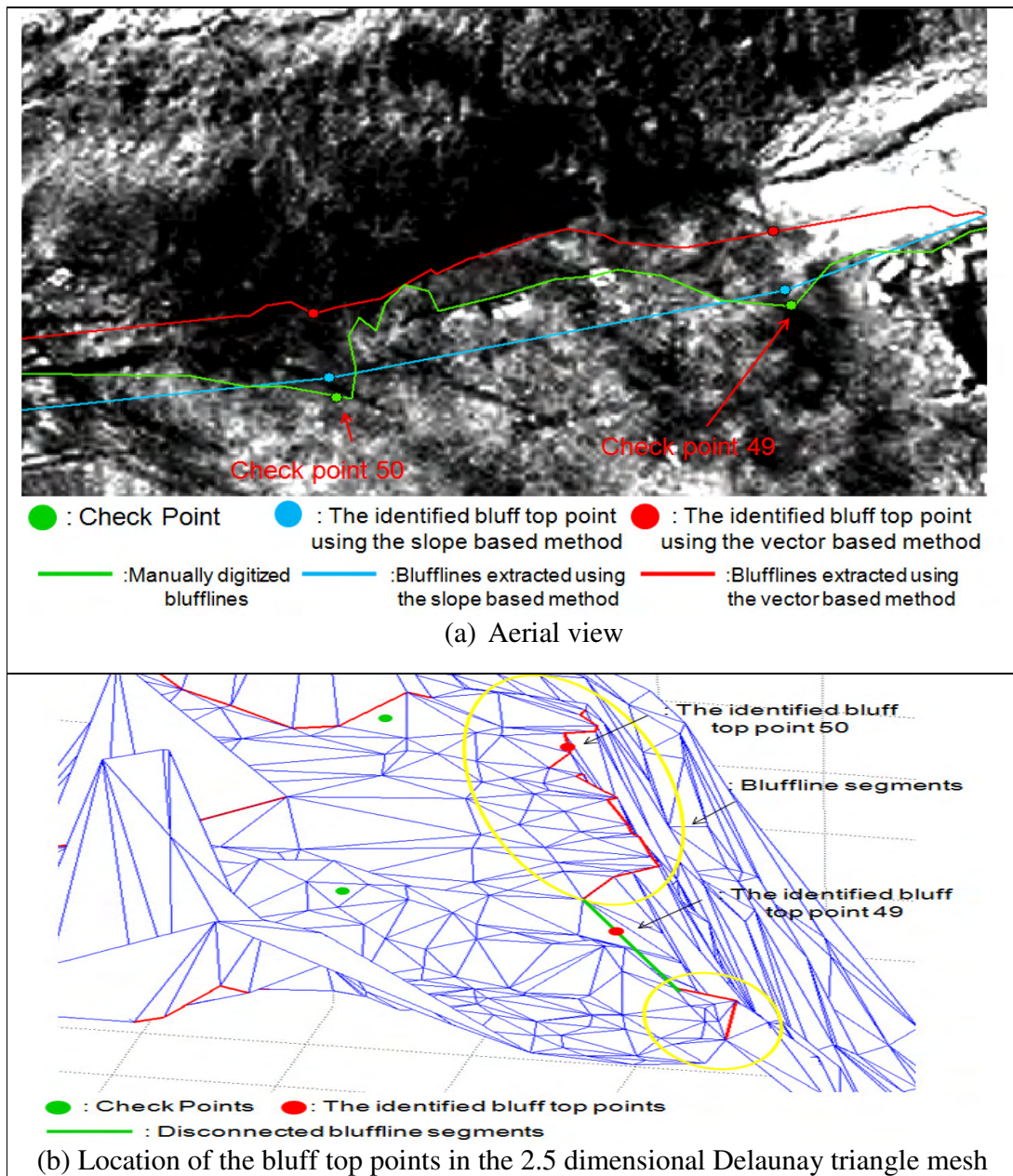Figure 4.17 The aerial view and the result of the identified bluff toe point using the slope based method with check point 22

In Figure 4.17(c), the maximum slope ($BSlope_{max}$) is extremely larger than any other slope values along the slope profile; hence, slope values of the points on the bluff toe are lower than the SC ($BSlope_{max}/4$). Thus, the points on the bluff toe cannot be selected as the multiple bluff toe candidates due to the extremely large maximum slope along the

slope profile. It causes the identified bluff toe point to have a horizontal and vertical outlier with check point 22.

Figure 4.18 shows the aerial view and the result of the identified bluff toe point using the slope based method with check point 36.

Figure 4.18 The aerial view and the result of the identified bluff toe point using the slope based method with check point 36

In Figure 4.18(c), due to tidal fluctuation near the shore, the LiDAR points in the red circles have a lower elevation in comparison to near LiDAR points on the water surface. Since the transect (the yellow line in Figure 4.18(c)) is located nearby the points in the red circles, some interpolated points, in the reversed elevation profile, located on the water surface also have higher slope values than the slope constraint due to these LiDAR points in the red circles. Thus, the bluff toe point is identified on the water surface due to tidal fluctuation near the shore.

In addition, the manually digitized bluffline is closer to the land than the extracted blufflines using both methods, and it causes check point 36 to have a higher elevation than the identified bluff toe points using both methods. We assume that the bluff toe line in the region has moved toward the land due to serious coastal erosion during the time period when the LiDAR data and the aerial orthoimages were taken. Thus, the identified bluff toe points using both methods also have vertical outliers with check point 36.

Figure 4.19 shows the aerial view and the result of the identified bluff toe point using the vector based method with check point 2.

(a) Aerial view

(b) Location of the identified bluff toe point in the 2.5 dimensional Delaunay
triangle mesh

Figure 4.19 The aerial view and the result of the identified bluff toe point using the vector
based method with check point 2

Figure 4.20 shows the aerial view and the result of the identified bluff toe point using the
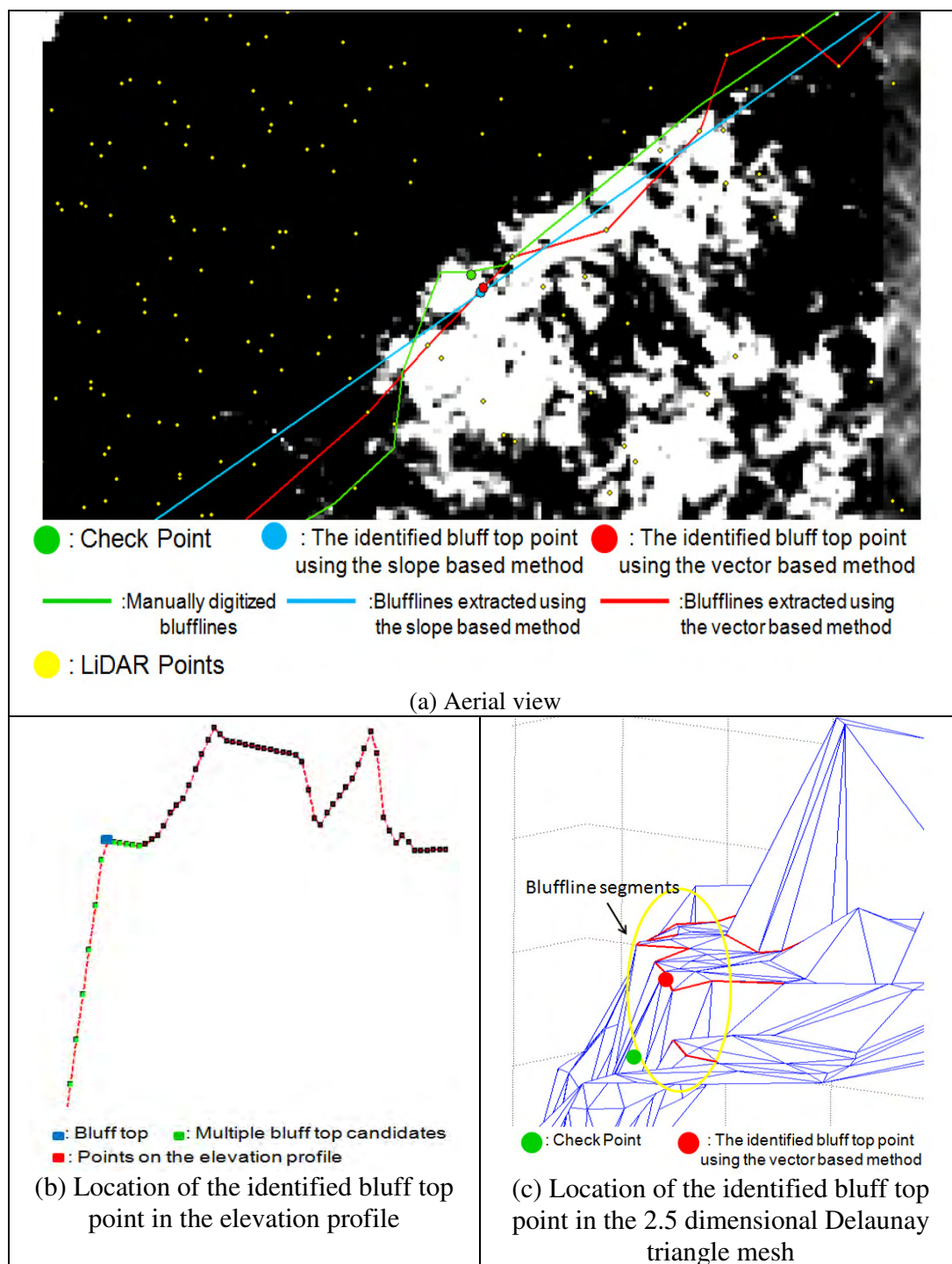
vector based method with check point 6.

(a) Aerial view

(b) Location of the identified bluff toe point in the 2.5 dimensional
Delaunay triangle mesh
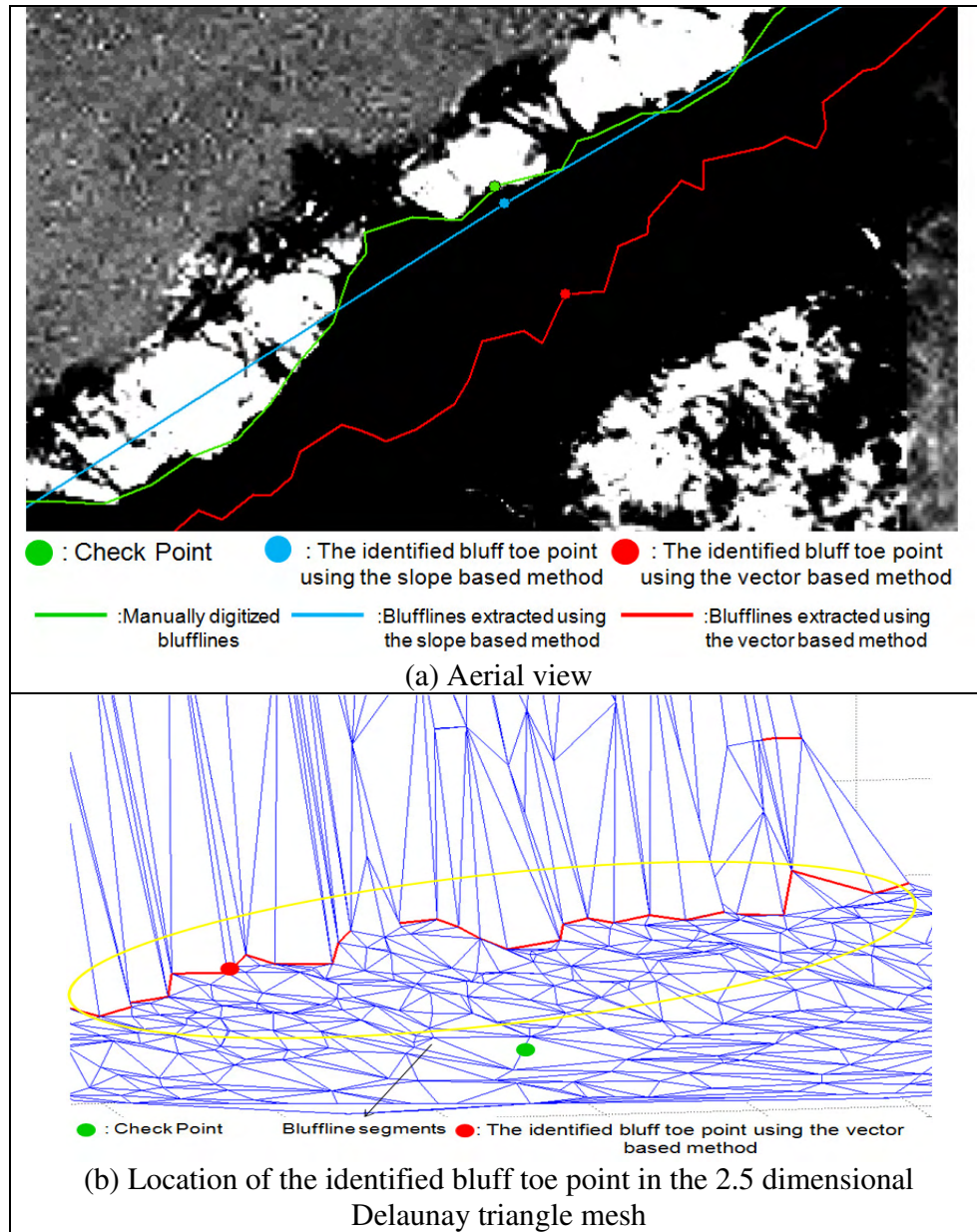
Figure 4.20 The aerial view and the result of the identified bluff toe point using the vector
based method with check point 6

Figure 4.21 shows the aerial view and the result of the identified bluff toe point using the

vector based method with check point 13.

74

: Check Point ● : The identified bluff toe point using the slope based method ● : The identified bluff toe point using the vector based method

──── :Manually digitized blufflines ──── :Blufflines extracted using the slope based method ──── :Blufflines extracted using the vector based method

(a) Aerial view

● : Check Point   Bluffline segments   ● : The identified bluff toe point using the vector based method

(b) Location of the identified bluff toe point in the 2.5 dimensional Delaunay triangle mesh

Figure 4.21 The aerial view and the result of the identified bluff toe point using the vector based method with check point 13

Using the vector based method, the bluffline segments are located at the sharp front of the bluff toe in most bluff region of the study area. If the bluff toe is identified on a smooth surface near the base of bluff region, the identified bluff toe points using the vector based method generally have horizontal outliers with the check points. As seen in Figure 4.19(b), Figure 4.20(b) and Figure 4.21(b), the check points are located on smooth surfaces near the bluff toe; hence, the identified bluff toe points using the vector base method have horizontal outliers with check points 2, 6 and 13.

Figure 4.22 shows the aerial view and the result of the identified bluff toe points using both methods with check point 25.

(a) Aerial view

(b) Location of the identified bluff toe point in the elevation profile

(c) Location of the identified bluff toe point in the 2.5 dimensional Delaunay triangle mesh
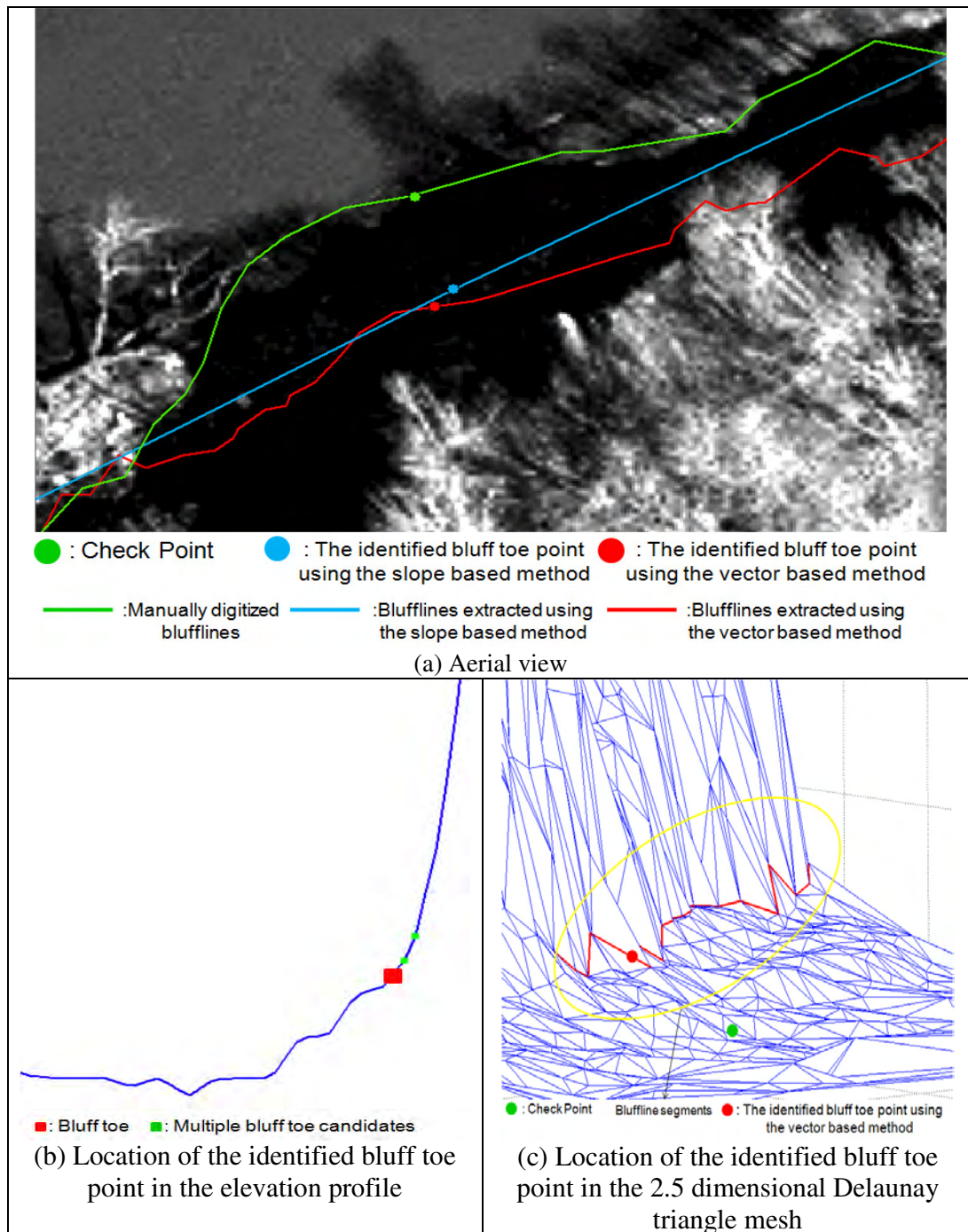
Figure 4.22 The aerial view and the result of the identified bluff toe points using both methods with check point 25

As seen Figure 4. 22(b) and (c), the identified bluff toe points using both methods are located at the sharp front of the base of bluff region; however, considering the aerial orthoimages, the check point is located on a smooth surface near the bluff toe. Thus, identified bluff toe points using both methods have horizontal outliers with check point 25.

Table 4.4 illustrates the measurement results of vertical accuracy of the two bluff toe lines, and Figure 4.23 shows the measurement results of the absolute vertical distance from the identified bluff toe point to each check point.

Bluff Toe	Maximum distance (meter)	Minimum distance (meter)	Average distance (meter)	Standard Deviation (meter)
Bluff toe extracted using the slope based method	6.110	0.005	0.655	1.141
Bluff toe extracted using the vector based method	4.099	0.001	0.565	0.797

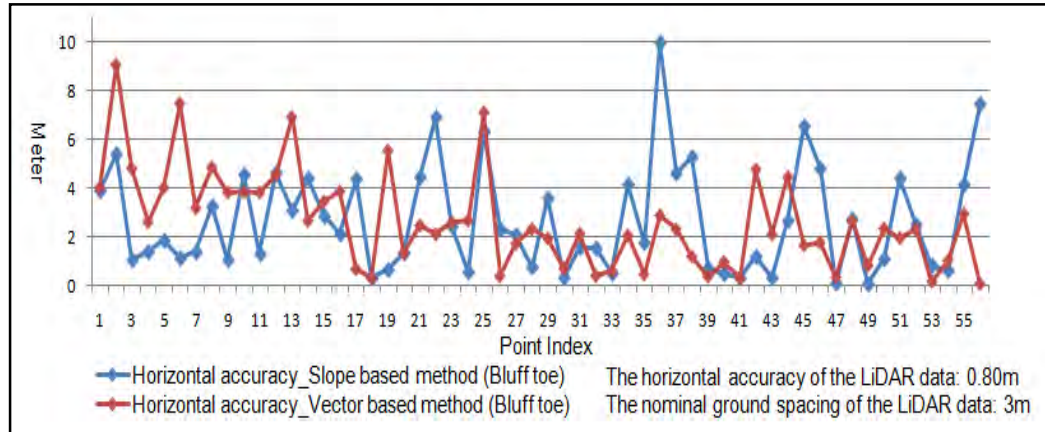Table 4.4 The measurement results of vertical accuracy of the two bluff toe lines
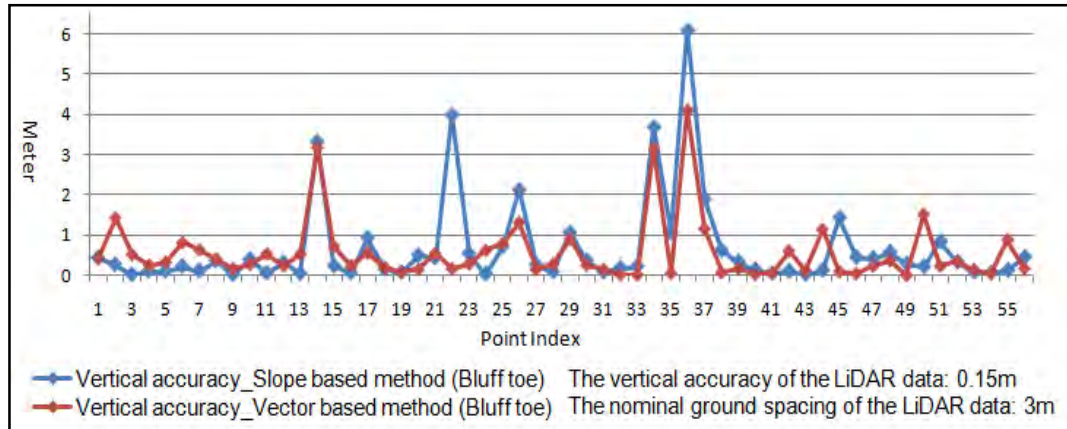
Figure 4.23 The measurement results of the absolute vertical distance from the identified bluff toe point to each check point

Reason for the vertical outliers of the identified bluff toe points using both methods is explained below.

1) We assume that the bluff toe line has moved landward due to serious coastal erosion during the time period when the LiDAR data and the aerial orthoimage were taken. These topographic changes cause the identified bluff toe points using both methods to have vertical outliers at some positions (The outliers with check points 14, 34 and 36).

Figure 4.24 shows the aerial view and the results of the identified bluff toe points using both methods with check point 14, and Figure 4.25 shows the aerial view and the result of the identified bluff toe points using both methods with check point 34.

79

(a) Aerial view

(b) Location of the bluff toe point in the elevation profile

(c) Location of the identified bluff toe point in the 2.5 dimensional Delaunay triangle mesh
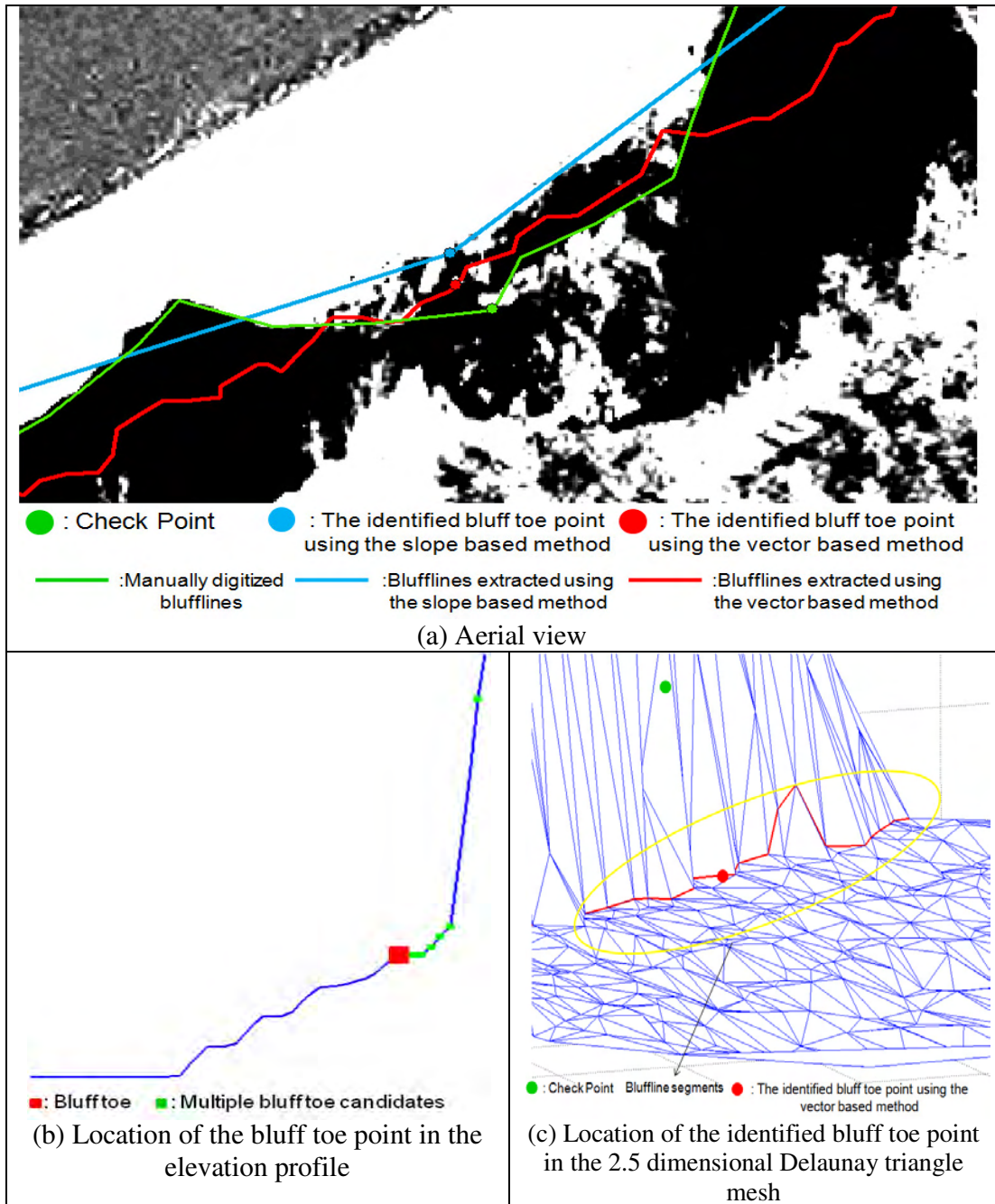
Figure 4.24 The aerial view and the result of the identified bluff toe points using both methods with check point 14

(a) Aerial view

(b) Location of the identified bluff toe point in the elevation profile

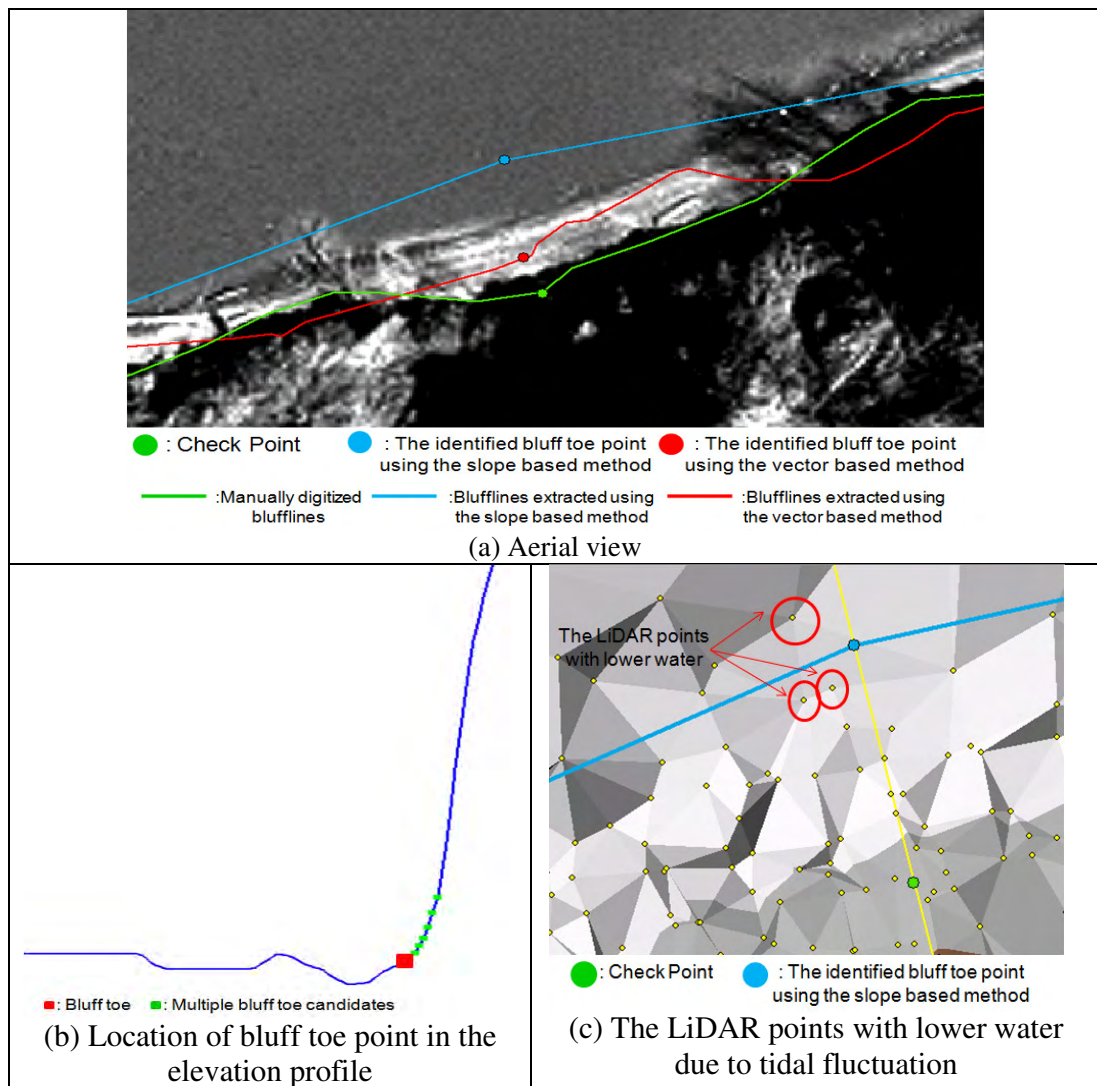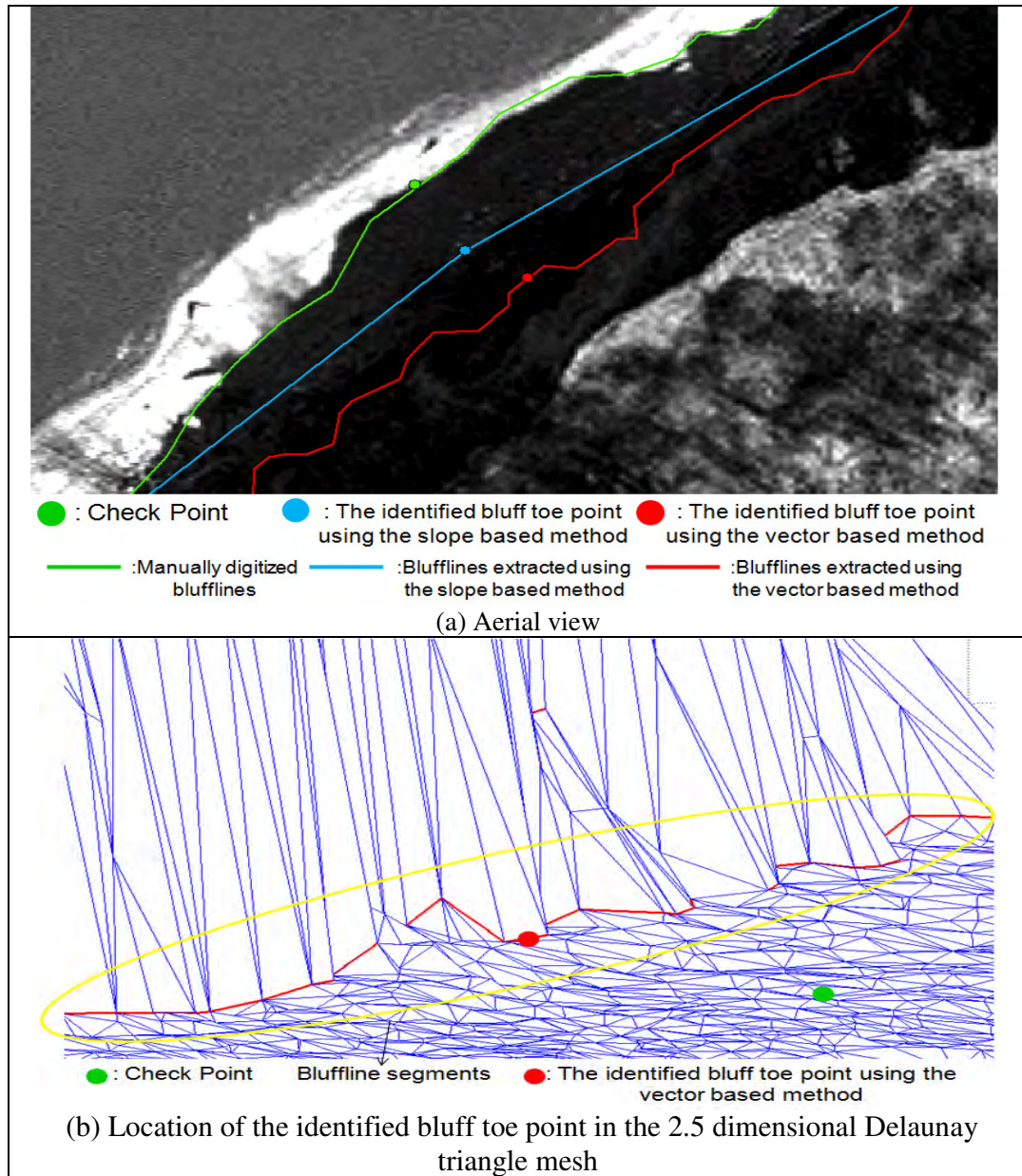(c) Location of the identified bluff toe point in the 2.5 dimensional Delaunay triangle mesh
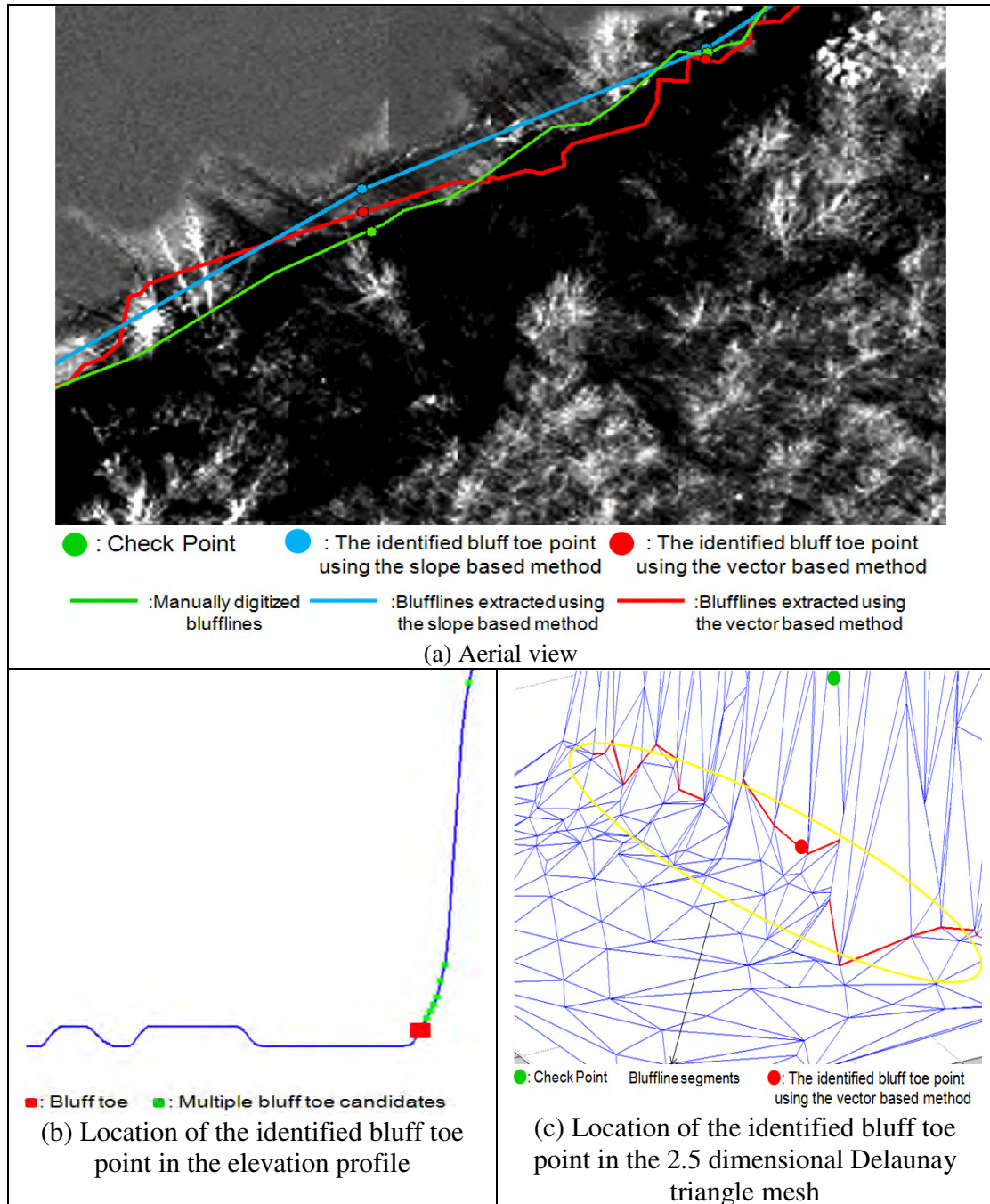
Figure 4.25 The aerial view and the result of the identified bluff toe points using both methods with check point 34

Figure 4.24(a) and Figure 4.25(a) shows that the manually digitized bluff toe lines are closer to the land than the extracted bluff toe lines using both methods. The identified bluff toe points using both methods have a similar horizontal and vertical location, and they are located on the bluff toe in the elevation profile and the 2.5 dimensional Delaunay triangle mesh. Thus, we assume that the bluff toe line has moved landward due to coastal erosion during the time period when the LiDAR data and the aerial orthoimages are taken, and it causes the identified bluff toe points using both methods to have vertical outliers with check points 14 and 34.

4.4 Conclusion

This section discusses conclusion of the measurement results and analysis of the measurement results of the extracted blufflines using both methods.

1) In general, the points located near the bluff toe have lower slopes than the points located near the bluff top, and they are usually located on irregular surfaces in the base of bluff region. Both methods, including the slope based method and the vector based method, analyze geometric patterns surrounding the blufflines and extract them from different aspects. The slope based method is employed to determine the bluff top and toe points by analysis of slope values of the points. The vector based method is employed to extract the bluffline segments by considering angle values defined by two normal vectors. Thus, due to the irregular location and lower slopes of the bluff toe, analysis of only geometric patterns

which surround the blufflines, does not provide enough information to detect the bluff toe.

2) Using the vector based method, numerous three dimensional bluffline segments are extracted, and they are connected to each other for generation of the three dimensional blufflines. However, using the slope based method, the bluff top and toe points are only identified along the transect; hence, extensive manual input is required to construct the three dimensional blufflines, such as creation of transects based on the LiDAR DSM, generation of the elevation profile along each transect and connection of each bluff top and toe points across transects. Thus, the vector based method has more automatic processes to extract the three dimensional blufflines than the slope based method.

3) Using the slope based method, the bluff top and toe points are determined by analysis of slope values of the points which compose the three dimensional elevation profile. These slope values are computed along the elevation profile in a single direction. This method does not consider three dimensional geometric patterns which surround the blufflines. Blufflines are located along the bluff top and toe, and their locations are affected by three dimensional geometric patterns. Thus, the slope based method does not provide enough information to extract the three dimensional blufflines due to its analysis of geometric patterns in a single direction.

4) Using the vector based method, angle values defined by two normal vectors are considered to extract the bluff edges which compose the bluffline segments. The

normal vectors are computed using the LiDAR points which compose the Delaunay triangle surfaces. Using the normal vector is an efficient technique to represent three dimensional geometric patterns in large surfaces, since it considers the locations of all points of the triangle surfaces. Thus, this method is a more efficient method to extract the three dimensional blufflines due to its analysis of three dimensional geometric patterns.

5) Considering that the LiDAR data and the aerial orthoimages were not taken at the same time, the location of the blufflines has changed at some positions during the time periods. Since the X and Y coordinates of the check points are obtained from the aerial orthoimages and the Z coordinates of them are obtained from the LiDAR data, this time period causes the extracted blufflines using both methods to have horizontal and vertical outliers with the check points at some positions.

6) The vector based method is useful for extraction of the bluffline segments located at the sharp front of the bluff top and the bluff toe. However, the vector based method has theoretical limitations to extract bluffline segments on a smooth surface near the bluff top and the bluff toe. Thus, in some areas where bluff region has the sharp front at the bluff top and the bluff toe, the vector based method can replace the slope based method for bluffline extraction; however, in some areas where bluff region has a smooth surface near the bluff top and the bluff toe, the vector based method cannot replace the slope based method for bluffline extraction. In addition, the extracted blufflines using the vector based method consist of not only the bluffline segments but also the disconnected

bluffline segments. If the identified bluff top or toe point is located on the disconnected bluffline segments, in general, the identified bluff top or toe point on the blufflines has an outlier with the check point. Most extracted linear features using the vector based method are located on the bluff top and the bluff toe; however, few linear feature edges are still located on vertical features or bluff face. Thus, further research is needed to remove all the linear feature edges which are not located at the bluff top and the bluff toe.

CHAPTER 5: CONCLUSIONS AND FUTURE WORK

In coastal studies, bluffline mapping is drastically important and essential for preservation of coastal properties, prediction of coastal erosion and estimation of shoreline movement. In this research, airborne LiDAR data is employed for extraction of the bluffline. Airborne LiDAR data is an efficient surveying data collection system for coastal mapping due to its advantages such as high vertical accuracy and capability to penetrate shallow water. For this research, a coastal zone of Lake Erie is selected as the study area where coastal erosion is serious.

The slope based method was developed and implemented in the Mapping and GIS lab of OSU. Using the slope based method, slope values of the points along the elevation profile are analyzed to detect the bluff top and toe points along each transect. This method has theoretical limitations to extract blufflines, since the method does not consider three dimensional geometric patterns to extract blufflines. In addition, since the bluff top and toe points are only identified alone each transect, a large amount of manual labor is required for generation of the three dimensional blufflines using the slope based method.

This thesis introduces a new vector based method for bluffline extraction using the LiDAR data. This method considers three dimensional geometric patterns to extract the three dimensional blufflines. Using the vector based method, angle values, defined by two normal vectors, are assigned to each edge, and they are considered for extraction of blufflines. Considering angle values, the line segments located at the bluff top and the bluff toe can be efficiently extracted by the vector based method. Using this method, the bluffline segments can be extracted in most bluff regions of the study area; hence, the method requires little manual work for construction of the three dimensional blufflines. Thus, this method is a more efficient method for bluffline extraction using the LiDAR data in comparison to the slope based method.

Blufflines extracted using only the LiDAR data have higher vertical accuracy than horizontal accuracy. In general, line structures extracted from the image sources such as the aerial orthoimages or the high-resolution satellite images have higher horizontal accuracy. Due to the complexities of coastal mapping and irregular surfaces of the coastal zone, no single type of surveying data can provide an efficient and reliable solution for complicated tasks of coastal mapping such as bluffline extraction. Hence, utilization of multiple remote sensing data including the airborne LiDAR data, the aerial orthoimages, and the high-resolution satellite images, etc. can provide additional information for bluffline extraction with higher accuracy.

Combined utilization of the airborne LiDAR data with the multiple image source data such as the aerial orthoimages or the high resolution satellite images would give reliable solutions for bluffline extraction with better accuracy in both horizontal and vertical

directions. Thus, data integration of the airborne LiDAR data with multiple image source

data would be a further research for bluffline extraction after this thesis.

REFERENCES

Ali, T., 1999. GIS modeling of phosphorus concentration, soil loss due to water erosion and coastal terrain change detection in Lake Erie coastal areas, Master Thesis, The Ohio State University, Columbus, Ohio.

Ali, T., 2003. New methods for positional quality assessment and change analysis of shoreline features, Ph.D. Dissertation, The Ohio State University, Columbus, Ohio.

Bebis, G., T. Deaconu, and M. Georgiopoulos, 1999. Fingerprint identification using Delaunay triangulation, *Proceedings of IEEE Conference on Information Intelligence and Systems*, pp. 452–459.

Briese, C., 2004. Three-dimensional modelling of breaklines from airborne laser scanner data, *International Archives of Photogrammetry and Remote Sensing,* Istanbul, Turkey, 35, B3, unpaginated CD-ROM.

Brock, J.C., C.W. Wright, A.H. Sallenger, W.B. Krabill, and R.N. Swift, 2002. Basis and methods of NASA Airborne Topographic Mapper Lidar surveys for coastal studies, *Journal of Coastal Research*, 18(1): 1-13.

Brown, E.A., C.H. Wu, D.M. Mickelson, and T.B. Edil, 2005. Factors Controlling Rates of Bluff Recession at Two Sites on Lake Michigan, *Journal of Great Lakes Research*, 31:306-321.

Brügelmann, R., 2000. Automatic breakline detection from airborne laser range data, *International Archives of Photogrammetry and Remote Sensing,* Amsterdam, Netherlands, 33, B3, pp. 109-115.

Buonaiuto, F.S., and H. Bokuniewicz, 2005. Coastal Bluff Recession and Impacts on Littoral Transport: Special Reference to Montauk, NY, *Shore & Beach,* 73(4): 24-29.

California Coastal Commission, 2004. Procedural guidance document: Monitoring attachments and glossary, URL: *http://www.coastal.ca.gov/pgd/pgd-mon2.html* (last date accessed: 04 October 2008).

Chopakatla, S.C., T.C. Lippmann, and J.E. Richardson, 2008. Field Verification of a Computational Fluid Dynamics Model for Wave Transformation and Breaking in the Surf Zone, *ASCE Journal of Waterway, Port, Coastal, and Ocean Engineering*, 134(2):71-80.

Fletcher, C., J. Rooney, M. Barbee, S.-C. Lim, and B. Richmond, 2003. Mapping Shoreline Change Using Digital Orthophotogrammetry on Maumi, Hawaii, *Journal of Coastal Research*, 38:106-124.

Gill, S.K., and J. R. Schultz, 2001. Tidal datum and their applications, U.S. Department of Commerce, National Oceanic and Atmospheric Administration, NOAA Special Publication NOS CO-OPS 1, 111p.

Harris, M., J. Brock, A. Nayegandhi, and M. Duffy, 2005. Extracting shorelines from NASA airborne topographic lidar-derived digital elevation models: Reston, Virginia, U.S. Geological Survey Open-File report 2005-1427. URL: *http://pubs.usgs.gov/of/2005/1427/* (last date accessed: 04 October 2008).

Hubeli, A., and M. Gross, 2001. Multiresolution Feature Extraction for Unstructured Meshes, *IEEE Visualization*, 21-26 October, San Diego, California, pp. 287 – 294.

Li, R., 1997. Geographical Information Systems for Shoreline Management – A Malaysian Experience, *1997 GIS/LIS Proceedings*, pp. 322-329.

Li, R., J.-K. Liu, and Y. Felus, 2001. Spatial Modeling and Analysis for Shoreline Change Detection and Coastal Erosion Monitoring, *Marine Geodesy*, 24: 1-12.

Liu, J.-K., 1998. Developing geographic information system applications in analysis of responses to lake Erie shoreline changes, Master Thesis, The Ohio State University, Columbus, Ohio.

Liu, J.-K., R. Li, S. Deshpande, X. Niu, and T.-Y. Shih, 2009. Estimation of Blufflines Using Topographic Lidar Data and Orthoimages, *Photogrammetric Engineering & Remote Sensing*, 75(1): 69-79.

Ma, R., 2004. Building model reconstruction from LiDAR data and aerial photographs, Ph.D. Dissertation, The Ohio State University, Columbus, Ohio.

Maine Geology Survey, 2009. Coastal Erosion Assessment for Maine FIRMs and Map Modernization Plan, URL: *http://www.maine.gov/doc/nrimc/mgs/explore/marine/ firms/summary.htm* (last date accessed: 20 August 2009).

Mayer, L.A., R.K. Barbor, P. Boudreau, T. Chance, C. Fletcher, H. Greening, R. Li, C. Mason, K. Metcalf, S. Snow-Cotter, and D. Wright, 2004. *A Geospatial Framework for the Coastal Zone National Needs for Coastal Mapping and Charting, Final report,* The National Academies Press, Washington, D.C., 149 p.

Mulchrone, K.F., 2002. Application of Delaunay triangulation to the nearest neighbour method of strain analysis, *Journal of Structural Geology*, 25(2002): 689-702.

NOAA, 2009. Remote sensing for coastal management, NOAA Coastal Service Center, URL: *http://www.csc.noaa.gov/crs/rs_apps/sensors/lidar.htm* (last date accessed: 10 August 2009).

O'Rourke, J., 1993. Computational Geometry in C, Cambridge University Press, Cambridge, 175 p.

Page, D.L., Y. Sun, A.F. Koschan, J. Paik, and M.A. Abidi, 2002. Normal Vector Voting: Crease Detection and Curvature Estimation on Large, Noisy Meshes, *Graphical Models*, 64: 199 – 229.

Schenk, T., 1999. Digital Photogrammetry: Volume I, TerraScience, Laurelville, Ohio, 422 p.

Shalowitz, A. L., 1964. Shore and Sea Boundaries, U.S. Department of Commerce, National Oceanic and Atmospheric Administration, National Ocean Service, 631 p.

Srivastava, A., 2005. A Least-Squares Approach to Improved Shoreline Modeling, Master Thesis, The Ohio State University, Columbus, Ohio.

Srivastava, A., X. Niu, K. Di, and R. Li, 2005. Shoreline modelling and erosion prediction, *Proceedings of ASPRS Annual Conference,* Baltimore, Maryland, unpaginated CD-ROM.

Tse, R.O.C., C.M. Gold, and D.B. Kidner, 2007. Building reconstruction using LiDAR data, *International Archives of Photogrammetry and Remote Sensing*, 28-29 August, Xingjiang, China, pp. 121-126.

Washington State Department of Ecology, 2009. Managing Drainage on Coastal Bluffs, URL: *http://www.ecy.wa.gov/programs/sea/pubs/95-107/glossary.html* (last date accessed: 26 May 2009).

Wozencraft, J.M., and D. Millar, 2005. Airborne lidar and integrated technologies for coastal mapping and charting, *Marine Technology Society Journal*, 39(3): 27-35.

Wright, C.W., and J. Brock, 2002. EAARL: A lidar for mapping shallow coral reefs and other coastal environments, *Proceedings of the Seventh International Conference on Remote Sensing for Marine and Coastal Environments*, 20-22, May, Miami, Florida.

Zuzek, P.J., B.N. Robert, and J.T. Scott, 2003. Spatial and temporal considerations for calculating shoreline change rates in the Great Lakes basin, *Journal of Coastal Research,* 38: 125-146.

APPENDIX A: COORDINATES OF THE CHECK POINTS

- Coordinates of the check points for the bluff top (feet)

Point Index	X coordinates	Y coordinates	Z coordinates
1	2319906.2352	770527.1802	618.585
2	2319827.6220	770469.1296	618.629
3	2319756.4451	770408.7814	616.801
4	2319691.3168	770332.2383	619.077
5	2319609.8403	770269.4164	619.285
6	2319540.4746	770204.2067	619.345
7	2319448.8059	770143.8202	611.998
8	2319290.5771	770028.8745	620.627
9	2319211.4772	769973.6336	619.547
10	2319137.1626	769898.8839	615.701
11	2319064.9301	769825.0798	620.251
12	2319002.7714	769785.8547	611.969
13	2318930.8698	769713.2939	623.429
14	2318855.4509	769627.7579	622.029
15	2318772.1938	769569.7330	619.585
16	2318679.0667	769542.7753	612.222
17	2318599.5135	769471.5877	618.974
18	2318529.7865	769401.2116	623.403
19	2318444.2990	769355.5458	618.607
20	2318359.3023	769305.6189	623.297
21	2318310.8282	769268.1086	621.568
22	2318126.6401	769146.8446	617.784
23	2317864.5462	768984.2590	621.742
24	2317764.2400	768948.9873	621.773
25	2317693.3840	768881.0380	621.934
26	2317520.1433	768764.2224	623.670
27	2317432.4981	768697.4780	624.167

Point Index	X coordinates	Y coordinates	Z coordinates
28	2317352.5467	768637.2408	628.410
29	2317280.4801	768581.6143	625.857
30	2317200.0308	768489.6555	624.652
31	2317108.5111	768426.8544	625.699
32	2317009.2810	768376.4694	629.243
33	2316917.2382	768334.1394	625.975
34	2316824.3025	768306.4205	625.821
35	2316750.1994	768271.5921	627.588
36	2316652.9743	768239.3564	627.630
37	2316555.9532	768200.8390	626.931
38	2316451.6366	768165.9216	629.338
39	2316364.9324	768172.1972	632.790
40	2316154.3053	768195.3080	626.726
41	2316090.1516	768146.7432	627.038
42	2316028.6435	768082.0283	627.504
43	2315955.5788	768018.2889	627.928
44	2315885.1400	767935.1572	628.878
45	2315780.7443	767900.0938	630.586
46	2315693.1178	767840.0905	626.450
47	2315626.8136	767761.6707	635.048
48	2315527.4858	767710.0747	629.493
49	2315432.2426	767683.2483	631.325
50	2315335.5438	767660.4506	631.973
51	2315226.3860	767667.7735	628.418
52	2315105.0707	767694.0398	627.817
53	2315019.8067	767769.7945	627.040

- Coordinates of the check points for the bluff toe (feet)

Point Index	X coordinates	Y coordinates	Z coordinates
1	2319879.0307	770578.7051	573.894
2	2319793.1998	770524.4775	573.537
3	2319726.6689	770441.3952	574.360
4	2319658.2303	770373.0385	574.486
5	2319509.8907	770241.0477	574.041
6	2319422.7368	770185.9818	572.374
7	2319259.8993	770070.3241	573.628
8	2319177.0596	770017.7075	573.766
9	2319102.0907	769946.4709	573.914
10	2319028.4200	769869.5548	573.320
11	2318967.2442	769818.7642	572.584
12	2318894.8716	769750.7730	573.665
13	2318814.3856	769682.1327	573.900
14	2318753.0539	769598.9790	585.920
15	2318657.6325	769570.1662	574.729
16	2318579.6259	769505.6866	575.281
17	2318506.3642	769446.2632	578.010
18	2318425.8002	769394.0900	575.867
19	2318327.7371	769359.0526	575.191
20	2318284.7419	769317.2714	575.731
21	2318192.8126	769254.2196	575.196
22	2318109.8081	769194.0237	575.457
23	2317931.9794	769080.1491	573.940
24	2317847.1899	769029.7350	573.554
25	2317744.9857	769000.6690	571.460
26	2317672.2431	768927.4916	581.037
27	2317579.0741	768870.8852	573.912
28	2317494.8038	768828.6756	573.473

Point Index	X coordinates	Y coordinates	Z coordinates
29	2317413.9413	768738.9856	577.061
30	2317331.2355	768682.5479	575.969
31	2317257.1558	768633.5488	573.210
32	2317169.5039	768577.2410	574.484
33	2317086.7266	768507.1339	575.255
34	2316995.3166	768452.1047	584.151
35	2316904.7892	768402.7940	577.680
36	2316812.4899	768354.8205	590.127
37	2316724.4875	768334.3743	578.430
38	2316628.9168	768307.2233	573.322
39	2316525.5376	768282.4675	573.550
40	2316436.2501	768287.1927	571.415
41	2316335.5517	768288.3740	571.888
42	2316235.6386	768302.5175	573.315
43	2316137.8805	768260.2168	577.048
44	2316054.8177	768206.6092	573.375
45	2315985.4893	768127.4408	574.625
46	2315914.9407	768061.7019	574.437
47	2315831.0470	768001.9865	575.358
48	2315751.0088	767944.7895	574.994
49	2315654.5943	767901.8138	572.898
50	2315572.1415	767864.0633	572.446
51	2315471.9104	767820.6333	572.460
52	2315392.4175	767782.4868	573.451
53	2315303.8309	767761.3397	572.629
54	2315205.6574	767768.9599	571.158
55	2315091.9319	767846.4018	574.914
56	2315014.8276	767880.0177	573.454

APPENDIX B: COORDINATES OF THE BLUFF TOP AND TOE POINTS ON THE BLUFFLINES, EXTRACTED USING THE VECTOR BASED METHOD

- Coordinates of the bluff top points on the bluff top line (feet)

Point Index	X coordinates	Y coordinates	Z coordinates
1	2319895.934	770530.3180	618.029
2	2319817.072	770472.1120	618.568
3	2319754.476	770413.2640	613.841
4	2319691.972	770335.1205	619.036
5	2319605.577	770273.2831	619.049
6	2319538.756	770206.2050	619.153
7	2319450.192	770142.4172	619.556
8	2319290.609	770029.4405	620.495
9	2319209.431	769979.0017	621.515
10	2319140.536	769895.7848	619.984
11	2319062.580	769827.0227	620.714
12	2319009.899	769784.6693	620.308
13	2318929.318	769714.4596	621.765
14	2318846.976	769635.1937	622.804
15	2318773.287	769572.2875	619.224
16	2318685.674	769538.3255	618.954
17	2318600.463	769469.9386	619.473
18	2318527.921	769403.9986	619.032
19	2318444.253	769353.5950	621.376
20	2318350.883	769314.8623	622.810
21	2318307.877	769284.7460	619.122
22	2318128.673	769145.1215	618.637
23	2317865.200	768989.3290	621.583
24	2317762.879	768950.5261	623.167
25	2317693.261	768877.8567	622.333
26	2317514.090	768767.5867	623.199
27	2317430.600	768699.2410	624.230

Point Index	X coordinates	Y coordinates	Z coordinates
28	2317349.959	768640.5367	627.055
29	2317278.627	768589.0305	624.751
30	2317195.177	768494.3604	622.973
31	2317107.208	768434.2870	623.827
32	2317006.513	768386.5617	626.483
33	2316910.247	768347.6009	625.852
34	2316826.738	768314.0045	625.463
35	2316744.094	768285.4222	624.544
36	2316652.640	768240.4260	625.618
37	2316554.614	768209.4357	625.259
38	2316451.571	768166.0175	627.829
39	2316364.916	768171.8533	628.949
40	2316153.855	768199.1351	625.441
41	2316089.978	768153.0784	626.879
42	2316026.664	768084.0765	627.447
43	2315958.849	768015.8905	627.662
44	2315883.655	767938.8441	628.113
45	2315778.386	767901.1608	628.639
46	2315697.598	767837.9357	628.676
47	2315627.947	767761.2820	634.895
48	2315522.415	767721.2569	629.588
49	2315428.436	767701.7291	629.513
50	2315330.455	767681.3390	629.328
51	2315226.013	767669.8215	628.164
52	2315103.853	767691.1565	628.950
53	2315021.962	767771.3213	625.852

- Coordinates of the bluff toe points on the bluff toe line (feet)

Point Index	X coordinates	Y coordinates	Z coordinates
1	2319885.235	770567.1453	575.285
2	2319813.953	770503.1841	578.211
3	2319738.293	770430.8598	576.037
4	2319661.858	770365.4167	575.304
5	2319518.797	770231.4398	575.096
6	2319436.113	770165.4583	575.036
7	2319267.746	770063.6312	575.706
8	2319190.189	770008.8340	575.066
9	2319111.089	769937.8651	574.445
10	2319029.398	769857.0871	574.190
11	2318975.121	769809.1607	574.323
12	2318909.196	769746.9631	574.433
13	2318830.987	769666.7270	575.627
14	2318746.085	769604.0375	575.528
15	2318660.844	769559.4385	577.068
16	2318582.603	769493.4671	576.044
17	2318506.731	769448.3542	576.188
18	2318426.385	769393.4291	576.462
19	2318341.068	769346.8250	575.456
20	2318286.371	769313.4271	576.209
21	2318196.424	769247.1128	576.960
22	2318113.948	769188.5978	575.986
23	2317939.933	769077.5312	574.876
24	2317853.640	769023.9809	575.577
25	2317748.735	768977.7291	574.045
26	2317672.147	768928.6231	576.741
27	2317578.755	768876.4117	574.386
28	2317496.202	768821.2800	574.389

Point Index	X coordinates	Y coordinates	Z coordinates
29	2317410.572	768744.2199	574.124
30	2317329.377	768683.6489	575.144
31	2317264.054	768633.1032	573.683
32	2317170.219	768576.2930	574.433
33	2317086.292	768505.3461	575.305
34	2316993.025	768458.3008	573.838
35	2316906.065	768402.2592	577.847
36	2316808.562	768363.3058	576.678
37	2316723.809	768341.8246	574.642
38	2316631.018	768304.0593	573.546
39	2316524.843	768283.2964	573.025
40	2316434.695	768284.5686	571.484
41	2316335.564	768287.5026	571.716
42	2316236.640	768287.0131	575.302
43	2316141.821	768254.6786	577.432
44	2316066.367	768197.7489	577.094
45	2315988.942	768123.4260	574.921
46	2315919.781	768058.7485	574.575
47	2315830.478	768002.8635	574.616
48	2315748.996	767953.1277	573.799
49	2315656.291	767899.8950	572.901
50	2315575.695	767857.3953	577.403
51	2315472.525	767814.3776	573.210
52	2315388.102	767788.5955	572.336
53	2315303.865	767760.9329	573.064
54	2315205.457	767765.7274	571.298
55	2315084.593	767840.2649	577.810
56	2315014.902	767880.0747	574.007

APPENDIX C: COORDINATES OF THE BLUFF TOP AND

TOE POINTS, EXTRACTED USING THE SLOPE BASED

METHOD

- Coordinates of the bluff top points extracted using the slope based method (feet)

Point Index	X coordinates	Y coordinates	Z coordinates
1	2319902.288	770534.8106	619.160
2	2319822.139	770478.0719	618.744
3	2319757.600	770407.1732	618.990
4	2319678.976	770347.3650	610.546
5	2319610.760	770268.1872	619.218
6	2319542.119	770202.5617	619.185
7	2319449.907	770141.8852	619.406
8	2319286.037	770035.0740	620.103
9	2319207.771	769978.2200	621.736
10	2319146.058	769887.5904	621.587
11	2319063.818	769826.6137	620.580
12	2319013.105	769776.4921	620.701
13	2318927.178	769717.3511	626.513
14	2318851.391	769633.2171	621.978
15	2318774.687	769566.5120	619.000
16	2318682.855	769537.7745	618.598
17	2318605.506	769462.8407	618.786
18	2318532.342	769397.2947	623.824
19	2318446.347	769351.3476	621.000
20	2318356.821	769310.0627	621.000
21	2318305.672	769278.2057	619.000
22	2318131.816	769133.1453	620.052
23	2317864.851	768984.6671	621.000
24	2317766.509	768943.1041	621.972
25	2317696.915	768873.9352	622.000
26	2317518.796	768767.7852	622.011
27	2317444.596	768673.2144	631.589

Point Index	X coordinates	Y coordinates	Z coordinates
28	2317352.986	768636.6025	627.925
29	2317281.186	768579.4194	624.682
30	2317198.986	768491.6887	622.972
31	2317106.252	768434.4110	624.292
32	2317008.914	768379.6872	627.996
33	2316915.669	768338.9082	625.977
34	2316824.499	768307.6324	625.000
35	2316748.883	768274.3303	626.260
36	2316651.279	768244.1012	629.075
37	2316555.787	768199.8725	626.000
38	2316452.827	768154.9364	628.353
39	2316366.637	768165.0823	639.911
40	2316156.099	768190.2927	626.000
41	2316094.760	768138.6030	627.000
42	2316027.473	768083.3508	626.468
43	2315962.027	768011.3142	627.000
44	2315881.582	767939.5365	626.886
45	2315790.962	767885.2535	629.913
46	2315700.579	767828.7687	628.000
47	2315627.927	767759.9104	632.890
48	2315519.547	767726.0114	628.000
49	2315431.107	767687.0780	632.424
50	2315333.910	767665.4225	630.959
51	2315229.269	767652.4545	636.217
52	2315105.743	767683.9999	628.012
53	2315018.614	767765.1662	628.000

- Coordinates of the bluff toe points extracted using the slope based method (feet)

Point Index	X coordinates	Y coordinates	Z coordinates
1	2319884.932	770567.426	575.281
2	2319802.53	770509.478	574.373
3	2319729.026	770438.886	574.343
4	2319661.091	770369.571	574.779
5	2319513.743	770236.430	574.342
6	2319424.558	770182.828	573.067
7	2319257.337	770074.000	573.293
8	2319183.745	770009.419	574.904
9	2319104.234	769943.837	573.899
10	2319037.811	769858.002	574.601
11	2318964.285	769821.797	572.724
12	2318905.310	769739.803	574.684
13	2318820.440	769674.123	574.000
14	2318744.987	769610.888	575.000
15	2318652.039	769577.568	574.000
16	2318583.146	769499.762	575.441
17	2318499.425	769458.771	575.000
18	2318425.374	769394.991	575.376
19	2318328.719	769357.201	575.000
20	2318286.693	769313.340	577.320
21	2318186.996	769267.598	573.805
22	2318117.488	769172.751	588.555
23	2317934.614	769072.690	575.690
24	2317846.569	769031.418	573.485
25	2317752.233	768981.299	573.761
26	2317669.086	768934.339	574.083
27	2317576.431	768877.129	573.103
28	2317495.667	768826.381	573.237

Point Index	X coordinates	Y coordinates	Z coordinates
29	2317408.748	768749.497	573.620
30	2317331.042	768683.560	577.143
31	2317259.245	768628.928	573.446
32	2317171.208	768572.564	575.064
33	2317086.487	768508.731	574.562
34	2316992.725	768465.419	572.046
35	2316903.759	768408.443	574.232
36	2316804.677	768386.495	570.080
37	2316718.907	768348.384	572.265
38	2316623.058	768323.458	571.335
39	2316524.863	768284.653	572.444
40	2316436.014	768288.727	571.000
41	2316335.809	768287.374	571.998
42	2316236.529	768298.761	573.014
43	2316137.585	768261.216	577.012
44	2316059.285	768199.156	573.752
45	2316000.268	768111.994	579.295
46	2315904.561	768073.490	573.000
47	2315831.310	768002.021	576.696
48	2315745.877	767952.064	573.136
49	2315654.748	767901.883	572.000
50	2315570.688	767867.332	571.774
51	2315465.542	767833.535	569.740
52	2315389.040	767789.908	572.408
53	2315304.670	767758.799	572.854
54	2315206.267	767767.046	571.000
55	2315093.027	767832.898	575.285
56	2315013.720	767904.374	572.000